Master of science

ASSESSMENT OF TRIBOLOGICAL PROPERTIES OF Ti_3C_2 AS A WATER-BASED LUBRICANT ADDITIVE

The graduate school

of the University of Ulsan

Department of Mechanical Engineering

Nguyen Thi Huong

ASSESSMENT OF TRIBOLOGICAL PROPERTIES OF Ti_3C_2 AS A WATER-BASED LUBRICANT ADDITIVE

Supervisor: Professor Koo-Hyun Chung

A thesis submitted in partial fulfillment of the requirement for the Degree of Master of Philosophy to the School of Mechanical and Automotive Engineering, University of Ulsan, Korea

By

NGUYEN THI HUONG

Department of Mechanical Engineering

University of Ulsan, Korea

November 2020

ASSESSMENT OF TRIBOLOGICAL PROPERTIES OF Ti_3C_2 AS A WATER-BASED LUBRICANT ADDITIVE

This certifies that the master's thesis of
NGUYEN THI HUONG is approved by

Committee Chairman:	**Prof. Doo-Man Chun**
Committee Member:	**Prof. Sung-Tae Hong**
Committee Member:	**Prof. Koo-Hyun Chung**

University of Ulsan, Korea

November 2020

ACKNOWLEDGEMENT

My deep gratitude goes first to Professor Koo-Hyun Chung who guided me through my graduate education and who shared the precious experience, which is my grant motivation in this research. Without his guidance, this thesis would not have been possible.

I would like to thank all members of my laboratory (Tribology and Surface Engineering Laboratory) for their assistance in technology as well as for providing necessary information regarding this study. Their friendliness and enthusiasm are the motivation for me to overcome difficulties in work.

A special grateful to my parents for their caring, mobilization and sacrifices that is a great encourage for me to complete this thesis successfully.

Ulsan, 28 December 2020

TABLE OF CONTENTS

LIST OF TABLES

LIST OF FIGURES

ABSTRACT

The concern about the pollution created by the use of oil based lubricants has inspired research on green tribology solutions. Among the environmental-friendly lubrication currently under development, water-based lubrication technology interest due to its economic and environmental benefits, such as low cost, cleaning performance, natural resource conservation, and environmental sustainability. However, water-based lubrication is often limited in practical tribological applications, mainly due to its low viscosity and corrosivity. In order to overcome these limitations and improve the properties of water-based lubricants, extensive efforts have been made over the past decades (e.g., coating, surface texturing on the surface of sample). Furthermore, investigations have been conducted on the use of additives without environmentally harmful compositions has been proposed to overcome the limitations of water-based lubrication. Recently, 2D layered transition metal carbides and nitrides, MXenes, have attracted attention as candidates in the lubricant field due to its multi-layer structure which can easily shearing in order to reduce the friction and wear in the tribological system when the sliding occurs.

In this work, the tribological properties of titanium carbides (Ti_3C_2), a type of MXenes, as an additive in water-based lubrication was experimentally investigated using a ball-on-disk tribotester. Experiment were performed using stainless steel ball and disk at boundary lubrication under various normal forces and Ti_3C_2 concentrations in water. Both friction and wear were found to decrease with increasing Ti_3C_2 concentration up to 5 wt%, and then increase when the concentration was larger than 5 wt%. The results suggest that Ti_3C_2 flakes hindered direct contact, particularly at the edges of the contact interfaces. It was further shown that the agglomeration of Ti_3C_2 flakes may mitigate the hindering when an excessive amount of Ti_3C_2 (e.g., 7 wt%.) was applied. The decrease in the friction coefficient and wear rate with 5 wt% of Ti_3C_2 concentration was approximately 20% and 48%, respectively. The outcomes of this work may provide useful information to understand the effect of Ti_3C_2 on the tribological characteristic of stainless steel under water-based lubrication.

1. INTRODUCTION

1.1 Background and motivation

Environmental degradation such as resource depletion, climate change, and pollution has become a growing concern in the last few decades. To overcome these problems to ensure a sustainable future, various green technologies have been under development. In particular, green tribology involves minimization of friction and wear, environment-friendly or biodegradable lubrication, reduction or even elimination of the lubrication, complete utilization of materials, biomimetic surface design, and tribology for renewable sources of energy, with the aim to save energy and materials and to minimize the harmful impacts on the environment and ecological balance [1]. Among the green tribology solutions currently under development, water-based lubrication technology, which potentially can replace conventional oil-based lubricants, has attracted considerable interest due to its economic and environmental benefits, such as low cost, cleaning performance, natural resource conservation, and environmental sustainability.

Water-based lubrication is often limited in practical tribological applications, mainly due to its low viscosity and corrosivity. In order to overcome these limitations and improve the properties of water-based lubricants, extensive efforts have been made over the past decades. For example, fundamental studies to understand the performance of water-lubricated journal bearings have been performed [2,3]. Tribological properties of various coatings with good lubricity in a water environment have also been investigated [4,5]. In addition, to enhance the tribological properties of the coatings in water-based lubrication, surface texturing, such as nanostructure, micro-dimples, and grooves, has been proposed [6-8]. Furthermore, investigations have been conducted on the use of additives to overcome the limitations of water-based lubrication [9]. Various nanoparticles, including copper (Cu) [10], diamond [11], titanium dioxide (TiO_2) [12], and silicon dioxide (SiO_2) [13], have been proposed as potential candidates for lubricant additives. Carbon-based nanomaterials, such as fullerenes [14] and carbon nanotubes [15], have also attracted considerable interest as additives for water-based lubrication. Particularly, graphene and its derivatives have recently been demonstrated as promising lubricant additives due to their low friction characteristics associated with weak interatomic interactions between layers, and chemical

inertness [16-18]. For example, when graphene oxide was added in water, it was observed that the friction coefficient was maintained approximately at 0.05 for up to 60,000 cycles without any significant wear [17]. It was demonstrated that the decrease in friction and wear may be associated with the formation of a tribo-film that can act as a protective coating [17,18]. Furthermore, considering that other two-dimensional (2D) layered materials, such as molybdenum disulfide (MoS_2) and hexagonal-boron nitride (h-BN), can provide low frictional properties [19-21], their tribological characteristics as additives for water-based lubrication have been explored [22,23].

Recently, 2D layered transition metal carbides and nitrides, MXenes, have attracted attention as candidates for solid lubricants [24,25]. MXenes is the latest representative of the MAX phase which is also known as layered early transition metal carbides and nitrides. Their general formula is $M_{n+}1AX_n$ (n = 1-3) where M represents an early transition metal. A represents an element from group 13 or 14 and X stands for carbon or nitrogen. Titanium carbide (Ti_3C_2), often denoted as $Ti_3C_2T_x$, where T is F, OH, and O, is one of the most extensively studied MXenes due to the potential for various applications [24]. It was shown that Ti_3C_2 may provide a significant reduction of friction and wear, attributed to the prevention of the direct contact and formation of a carbon-rich tribo-film at the contact interface [26]. The tribological properties of Ti_3C_2 were further correlated with the surface terminations and intercalated water [27]. In particular, a practical approach for the use of Ti_3C_2 as solid lubricant for thrust ball bearings was conducted [28]. Furthermore, it was demonstrated that Ti_3C_2 can be exploited as a lubricant additive to oil-based lubricants [29-32]. However, the feasibility of Ti_3C_2 as an additive for water-based lubrication has not yet been thoroughly assessed.

1.2 Objective of the thesis

In this work, the tribological properties of Ti_3C_2 as an additive in water-based lubrication was experimentally investigated using a ball-on-disk tribotester. Experiments were performed using stainless steel (SS) ball and disk at boundary lubrication under various normal forces and Ti_3C_2 concentrations in water. The variation in friction was monitored during the tests and the wear rates of the specimens were quantitatively assessed using a laser scanning confocal microscope (LSCM) after the experiments. A

better understanding of the wear behavior with Ti_3C_2 additives was additionally pursued using scanning electron microscope (SEM) observations. The outcomes may provide useful information to understand the effect of Ti_3C_2 on the tribological characteristic of SS under water-based lubrication.

1.3 Organization of the thesis

The overall structure of this thesis taken the form of five sections, where the motivation and the objectives of this work have been explained so far in section 1. Section 2 will present the theory of basic related to this research that has been published so far. It begins from the general background of knowledge on friction and wear. The theoretical calculation of contact mechanics between sphere and flat surface and the describes related to lubricant theory are also mentioned. The experimental details including the materials and methods are given in section 3. The results of friction and wear of two material pairs sliding against each other and discussion of the lubricant and wear mechanisms of Ti_3C_2 as an additive were presented in section 4. Then, section 5 concludes the finding of this work. By recognizing the limitations, a few recommendations were discussed for further investigation.

2. THEORETICAL BASIC

2.1 Friction

2.1.1 Amontons friction law

Friction is a resistance force to tangential motion between two surfaces in a contact. The laws of friction were published by Guillaume Amontons which stated that the friction force is proportional to the normal load applied and independent of the apparent area of contact . The friction force, F can be stated by the basic equation:

$$F = \mu N \tag{2.1}$$

Where μ is called the coefficient of friction (COF) and N is the normal force.

2.2.2 Tribotester and friction force measurement

Prior to performing a tribological research, it is very important for a researcher to understand the system of pin-on-disk tribotester. The basic set-up in friction force measurement for a tribotester is by applying a normal load between two contacting bodies that have a relative motion (one body is moving while the other partner is static). The normal force then should be adjustable so that it could be increased gradually until a measurable tangential force is detected by a force measurement device. A calibrated load cell is normally attached to the static body as a friction force measurement device. The friction coefficient is then calculated by dividing the friction force F by the value of normal force N.

2.2.3 Friction mechanism during running-in period

Running-in is a process of changes in friction and wear in tribo system prior to steady state when two contacting surfaces are in contact under a normal force and relative motion. The running-in process is an effective way of matching two contacting components and gives importanct clues to system designer for identification of various contributions to overall friction performance of machines. The three attributes of frictional runnin-in behavior have been describesd in detail previously [33]. They are the duration of certain characteristic transients within the running-in period, including the time the reach steady-state, the general trend of the friction force corresponding with time of operation and the

instantaneous level of friction fluctuations superimponsed upon the general trend. There are eight common shapes of running-in behavior (friction-time curves) in metal sliding contact that were categorized by Blau [34] as showed in Figure 1. Table 1 indicates some of the possible causes for each type of curve. From the outcome of his research, it can be concluded that there was no evidence that these eight curves were representative of specific contact conditions [35].

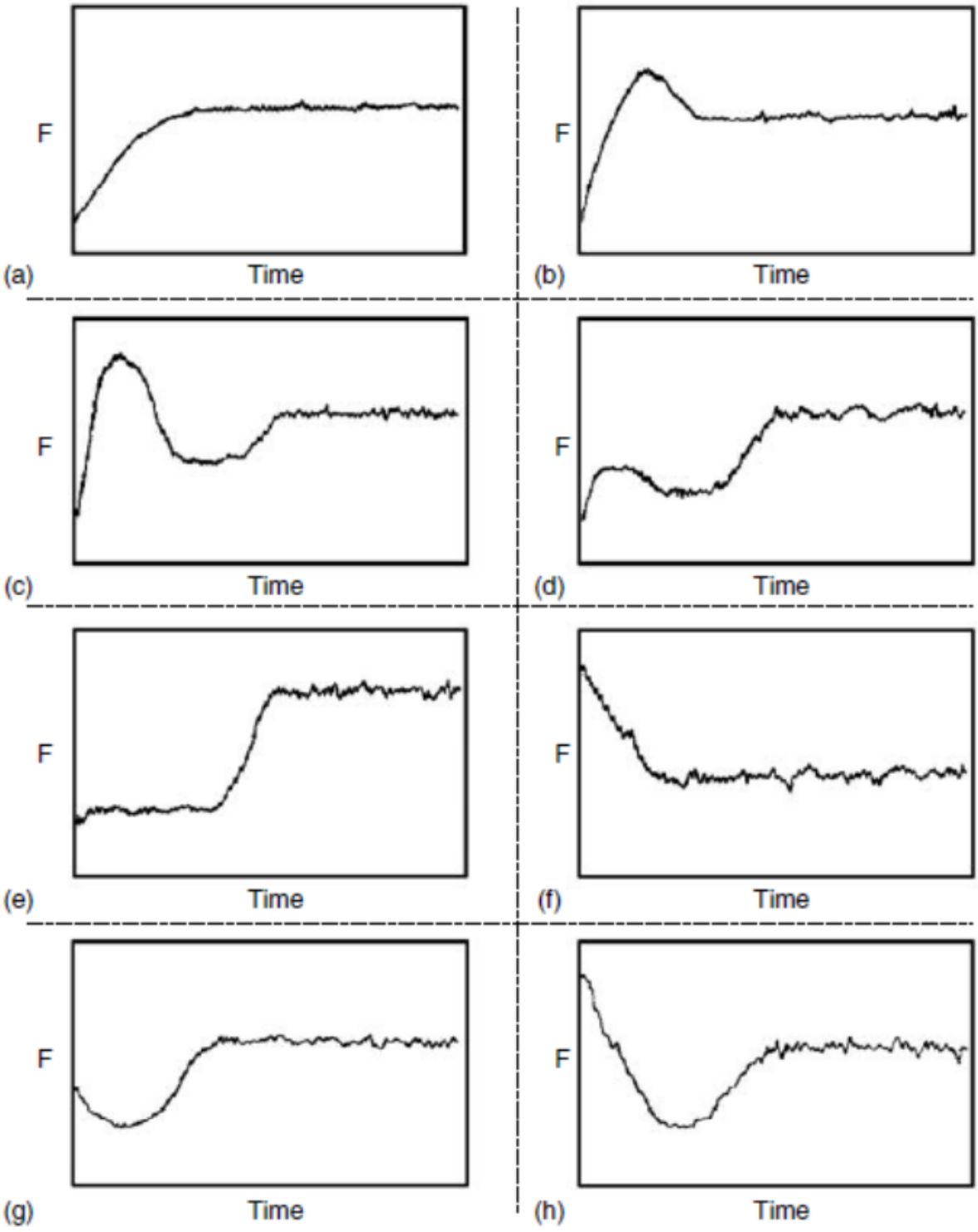

Figure 1. Eight typical forms of initial friction behavior during running-in process

Table 1. Eight typical forms of initial friction behavior during running-in process

	Occurrence	Possible cause
a	Contaminant surfaces	A thin film of lubricious contaminant is worn off the sliding surface [35]. Effects of component temperature rises due to sliding friction [36]. Mechanical disruption of surface oxide films with increasing metallic contact [37]
b	Boundary-lubricated metals	Surface wear-in; initial wear rate high until the sharpest asperities are worn off and surface becomes smoother [38].
c	Unlubricated oxidized metals, often observed in ferrous or ferrous/nonferrous pairs	Wear -in, as in type (b), but with the subsequent development of a debris layer (debris accumulation) or excessive transfer of materials [38].
d	Same as type (c)	Similar to type (c), but the initial oxide film maybe more tenacious and protective [38].
e	Coated systems; also, systems in which wear is controlled by subsurface fatigue processes.	Wear-through of a coating; or substrate fatigure cracks grow until debris is first produced. The debris then creates third bodies, which include a rapid transition in friction. Sometimes a few initial spikes in friction signal the onset of this transition [39].
f	Clean, pure metals	Crystallographic reorientation of regions in near surface layers reduces their shear strength and lowers their friction. Alternatively, the initial roughness of the surface is worn off, leaving smoother surface [35].
g	Graphite on graphite metal on graphite	Creation of a thin film during running-in, debris or transfer produces a subsequent rise in friction [35].
h	Hard coating on ceramics	Roughness changes, then a fine-grained debris layer forms [40].

2.2 Wear

2.2.1 Archard's wear law

Wear can be defined as progressive loss of substance from the operating surface of a body occurring as a result of relative motion at the surface. The basic theoretical establishment of Archard's wear law is given as follows [41]

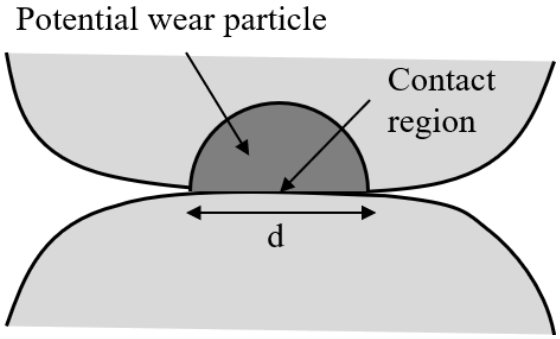

Figure 2. Hypothetical model of a hemispherical wear particles

Assume that two bodies sliding under an applied load L and call the flow pressure of the softer of the metals p, then the real area of contact will be given by

$$L = p \times A \tag{2.2}$$

Using hemispherical model (n contacting asperities) and assume that all the junctions are the same size, circles of diameter d and the total number n present at any instant will be given by

$$A = n \times \frac{\pi d^2}{4} \tag{2.3}$$

Hence

$$n = \frac{4A}{\pi d^2} = \frac{4L}{\pi p d^2} \tag{2.4}$$

Each junction may be assumed to remain in existence during a sliding distance equal to d, after which it is broken, and its load-carrying capacity is taken up by a new junction. Thus, the total number N of junctions formed in a sliding distance x is given by

$$N = \frac{nx}{d} = \frac{4Lx}{\pi p d^3} \tag{2.5}$$

The probability that any junction leads to the formation of a transferred fragment has been postulated to be equal to k, and, on the assumption that such a fragment is a hemisphere of diameter d, the volume V of wear per distance x of sliding is given by the relation

$$V = \frac{kN\pi d^3}{12} = \frac{kLx}{3p} \tag{2.6}$$

Because k is wear coefficient, so the wear volume can be re-write as:

$$V = \frac{kLx}{p} \tag{2.7}$$

2.2.2 Wear measurement methods

Wear is involving progressive loss of material and thus, mass loss is frequently used as a measure of wear. This is performend by measuring the mass of a spacimen before and after test. Other than mass loss measurement, calculation of wear volume could also be performed based on geometry of the wear scar of a worn specimen (length and width) which measured by laser scanning confocal microscopy (LSCM). Then, wear rate was calculated by wear volume divided by normal force multiplying with sliding distance.

2.2.3 Wear mechanisms

Wear initiates when there is insufficient protection between two contacting surfaces. The process by which wear occurs on the surfaces is commonly known as the wear mechanism. There are four main classes of wear mechanisms namely: adhesive wear, abrasive wear, corrosive wear and fatigue wear from [41].

2.2.3.1 Adhesive wear

Adhesive wear occurs when two smooth bodies are slid over each other, and fragments are pulled off one surface and adhere to the other. Later these fragments may come off the surface on which they are formed and be transferred back to the original surface, or else form loose wear particles.

In order for the adhesive wear to take place, fracture must occur in the subsurface of one of the materials (Figure 3) [42]. The formation of transfer films is a characteristic feature of adhesive wear where material is transferred from one surface to another before being released as a wear particle (Figure 4) [43]

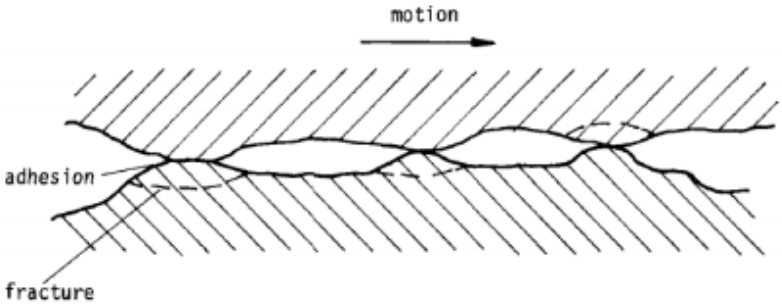

Figure 3. Formation of fracture in the subsurface of materials due to adhesive wear

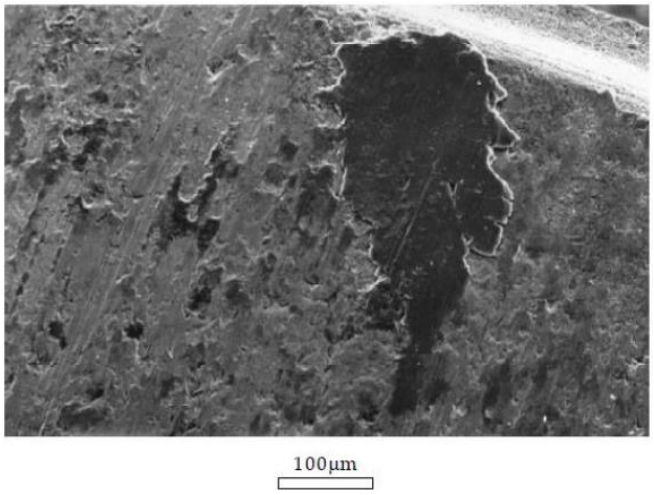

Figure 4. Example of adhesive wear appearance (Al-Si alloy transfer film onto a piston ring)

2.2.3.2 Abrasive wear

Abrasive wear occurs when a rough hard surface, or a soft surface containing hard particles, slides on a softer surface and ploughs a series of grooves in it. The material from the grooves is displaced in the form of wear particles, generally loose ones. In one case the hard particles are abrasives, in other case they are small adhesive particles pulled out the harder surface, transferred to the softer surface, and now scratching the harder surface. When abrasive wear is produced by the hard particles, it is called three-body abrasive, while two-body abrasive is caused by a harder asperities penetrating into a softer material (Figure 5) [44]. In abrasive wear, material is removed by a ploughing or microcutting process which is influenced by factors such as particles size, shape and material hardness. A typical appearance on a worn surface caused by abrasive wear is shown in Figure 6 [42].

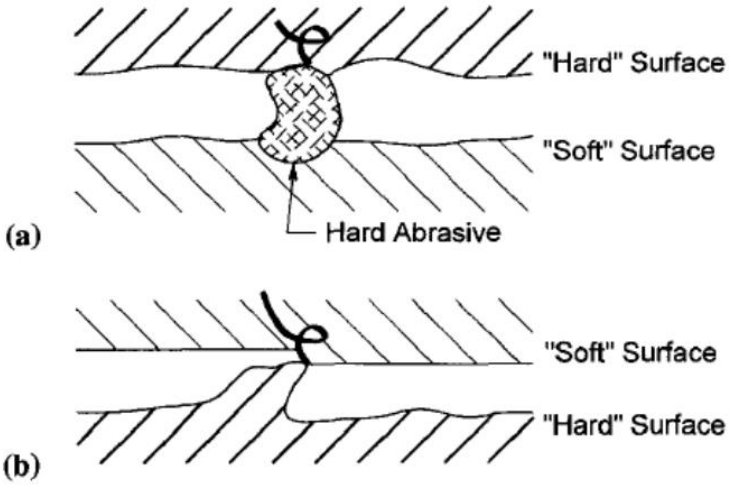

Figure 5. Schematic of three-body and two-body abrasive wear model

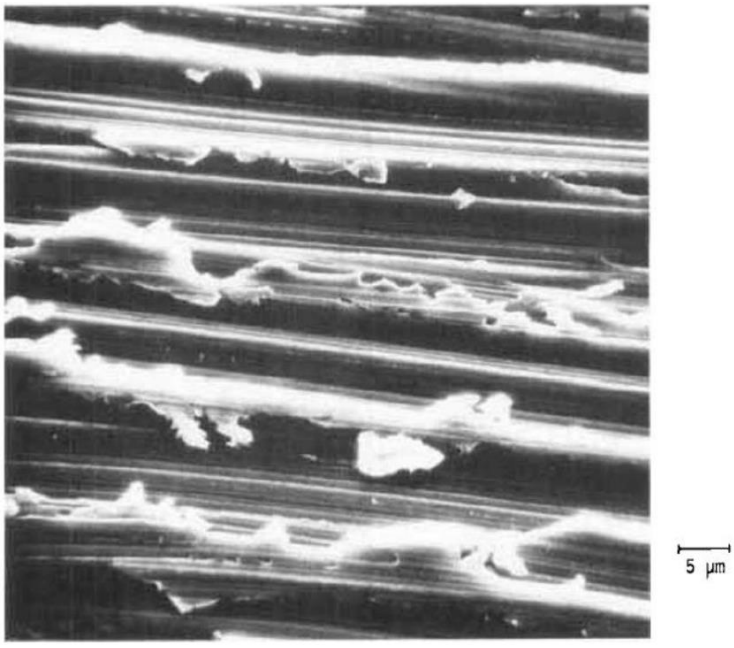

Figure 6. Example of abrasive wear appearance

2.2.3.3 Corrosive wear

Corrosive wear occurs when sliding takes place in a corrosive environment. In the absence of sliding, the products of the corrosion will form a film on the surfaces. This film tends to slow down or even arrest the corrosion. However, the sliding action wears the film away, so the corrosion attact continues. The mechanism of corrosive wear is shown in Figure 7 in which pitting is normally produced on the worn surface [45].

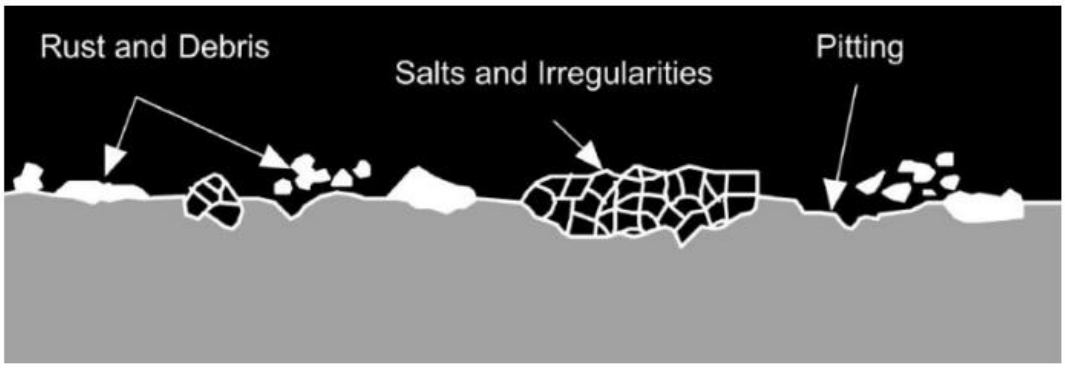

Figure 7. Mechanism of corrosive wear

2.2.3.4 Fatigue wear

Due to repeated sliding or rolling, cracks are formed at the surface or substrate, relatively larger wear particles are generated abruptly. Contrast to adhesive and abrasive wear, fatigue wear may be more significant after a certain degree of relative motion as shown in Figure 8 [43].

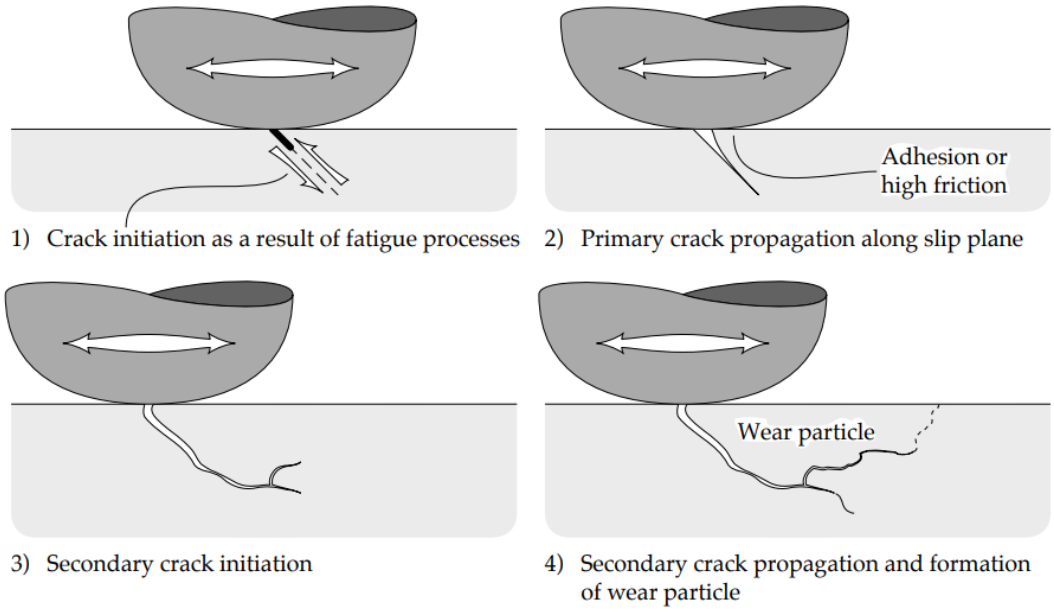

Figure 8. The process of surface crack initiation and propagation

2.3 Contact mechanics

Contact of surfaces occurs in all interfaces that transmit force or motion, or both. Hertzian contact refers to frictionless contact between two elastic bodies [46].

Sphere on sphere contact, $R_1 = R$, $R_2 = \infty$,

$$a^3 = \frac{3PR}{4E'} \tag{2.8}$$

If δ increases, contact radius increase $\delta \infty a^2$

$$\delta = \frac{a^2}{R} = \frac{\pi a^2}{\pi R} = \frac{A}{\pi R} \tag{2.9}$$

Contact area, $A = \delta \pi R$

From equations (2.8) and (2.9):

$$\delta = \left(\frac{9P^2}{16E'^2R}\right)^{1/3} \tag{2.10}$$

The contact pressure,

$$P = \frac{4}{3}E'R^{1/2}\,\delta^{3/2} \tag{2.11}$$

$$\frac{1}{E'} = \frac{1-v_1^2}{E_1} + \frac{1-v_2^2}{E_2} \tag{2.12}$$

Where E_1 and E_2 are the elastic moduli and v_1, v_2 the Poisson's ratios aassociated with each body.

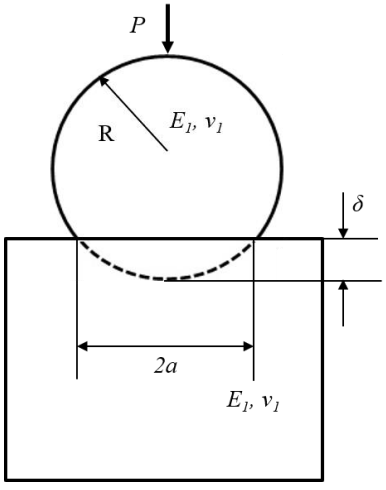

Figure 9. Hertzian contact model: sphere on plate

2.4 Lubrication

2.4.1 Lubrication regimes

In order to reduce friction and minimize wear between two contacting materials, a lubricant is applied to the contacting surfaces. A lubrication reduces the friction by providing a low shear strength layer between both surface which is less than the material shear strength. Lubricants operate under three common lubricating regimes that comprise of hydrodynamic, mixed and boundary lubrications. A summary of lubrication regimes can be explained by the Stribeck curve (Figure 10) [47] which is a plot of a fluid-lubricated bearing system that presents the coefficient of friction versus (ηN/P), where η is the lubricant viscosity, N is the rotational speed, and P is pressure.

Hydrodynamic known as full film lubrication when the contacting surfaces is fully supported by a relatively thick film. The mixed lubrication regime deals with lower speed, higher load or higher temperature that significantly reduces lubricant viscosity. Under this condition, the asperities of the contacting surfaces at some areas will occasionally in to contact. In boundary lubrication, the lubricant film thickness is thinner than height of asperities and there is considerable asperity contact. Boundary lubrication represents a more severe contact condition compared to other lubrication regime. Under this lubrication condition, the physical and chemical properties of thin surface films are significant.

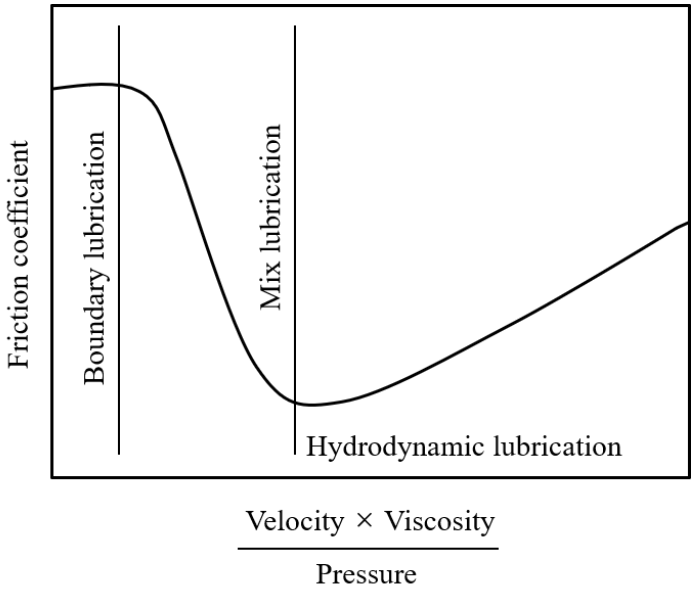

Figure 10. Stribeck curve showing different lubrication regimes

2.4.2 Two-dimensional materials as lubricant additive

2D materials are defined as materials that are crystalline and consist a single layer of atomes, 2D materials can generally be categorized into either 2D allotropes of various elements or compounds as a suspension of graphite oxide with atomic planes. Properties such as conductivity of heat and electricity, corrosion resistance, optically transparent, and flexibility makes 2D materials ideal for usage in various of application fields. The 2D materials investigated as lubricant additive can be roughly divided into three categories: graphene family, metal dichalcogenides and others [48]. However, in this thesis scope, MXenes was emphasized.

2.4.2.1 Graphene family

To date, graphene is the thinnest artificial material know to the scientific community. It consists of carbon atoms with a layer thickness of only 0.335 nm. These sp^2 – bonded carbon atoms are tightly arranged in a 2D hexagonal structure known as a honeycomb and endow graphene with unique thermal, electrical, mechanical, and tribological properties such as extreme strength and seasy shear capability. Furthermore, its large surface area and layered structure also allow it to readily enter the contact interface of a tribo-pair, preventing the direct contact of rough surfaces and reducing friction and wear. The potential of graphene to reduce energy waste and increase the duability and reliability of mechanical assemblies has benn demonstrated when even a very small amount of graphene is supplied between rubbing surfaces [49,50]

2.4.2.2 Transition metal dichalcogenides (TMDCs)

TMDCs are a structurally and chemically well-defined family with a chemical formula of MX_2, where M stands for the transition metal element and X represents a chalcogen (S, Se, or Te). The 2D morphology of MX_2 materials ends them low shear resistance to any applied shear stress and decreases friction at the interface. MoS_2 is a typical representative TMDC which has garnered a great deal of research interest.

2.4.2.3 MXenes

MXenes is a 2D material, group of early transition metal carbides or carbonitrides. These are produced by the etching out of the A layers from MAX phase with hydrofluoric acid, and ending up with 2D layers of $M_{n+1}X$ terminated with OH/F groups [51,52]. $M_{n+1}AX_n$, where M is an early transition metal, A is mainly a group IIIA or IVA (i.e., groups 13 or 14) element, X is C and/or N, and n = 1, 2, or 3. The MAX phase structure can be described as 2D layers of early transition metal carbides and/or nitrides "glued" together with an A element as shown in Figure 11 from [47]. Because the M-A bonds are weaker than the M-X bonds heating of MAX phases under vacuum at high temperatures results in the selective loss of the A element. Today, MXene family includes Ti_3C_2, Ti_2C, Nb_2C, V_2C, $(Ti_{0.5},Nb_{0.5})_2C$, $(V_{0.5},Cr_{0.5})_3C_2$, Ti_3CN, and Ta_4C_3 [52,53]. Because the n values for the existing $M_{n+1}AX_n$ phases can vary from 1 to 3, the corresponding signle MXene sheets consist of 3, 5 or 7 automic layers for M_2X, M_3X_2, and M_4X_3, respectively.

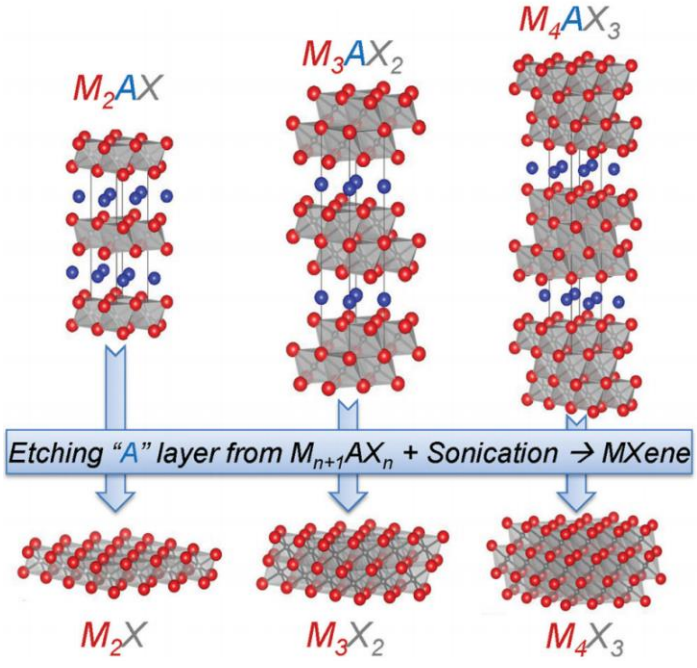

Figure 11. Structure of MAX phases and the corresponding MXenes

2.4.3 Role of 2D materials in friction and wear reduction mechanisms

Numerous studies have been made to understanding the underlying mechanisms of 2D materials as lubricant additive in effort to promote their wider application. Generally, the evolution of the protection of the lubricants can be divided into jour aspects: entering the contacting area of sliding surfaces; tribo-film formation; filling the grooves of the contact area and affectin the fluid drag and viscosity. The four proposed mechanisms are schematically expressed in Figure 12 [48].

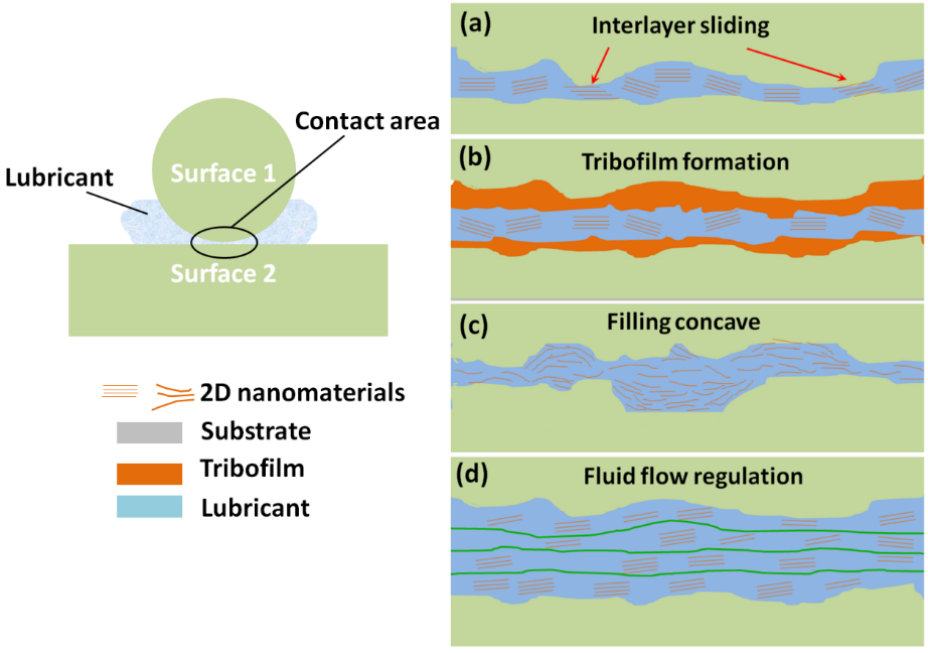

Figure 12. Possible mechanisms of 2D nanosheets to reduce friction and wear.

2.4.3.1 Entering the contacting area of sliding surfaces and providing efficient lubricating

2D materials have a multilayer structure and small size, when the sliding occurs, such particles can be easily enter into the rubbing contact. The introduction of nanoparticles in 2D materials further enhanves their penetration into the interspaces of contact surfaces, which makes lubrication possible. When two contacting surfaces sliding against each other under normal force, the 2D nanomaterials in the contact area subjected to normal pressure as well. The relative motion of the contacting surface supplies a shear stress to these materials. As a results, the easy shearing of interlayers in the multilayer 2D material forms a sliding system with the rubbing contact [16].

2.4.3.2 Tribo-film formation

The formation of a tribofilm can occurs at the contacting area of sliding surfaces in two stages of lubrication. At the initial stage, high surface energy and easy shearing allow them to easily adsorb onto the surface of the substrate to form a conformal protective film in the absence of any chemical reactions. In this stage, the protective film mainly severs to separate the two contacting surfaces. It prevents direct contact between the two sliding surfaces and reduces the friction and wear.

2.4.3.3 Filling the grooves of the contacting area

Due to the inherently limited manufacturing techniwues, no tribopair is completely smooth. The interface is uneven at the micro scale. Macro-asperities can produce high contact pressure during rubbing process. 2D nanomaterials, particularly those anchored with nanoparticles, can fill in grooves areas on the rubbing surfaces to smooth them [48]. A smoother surface processes less asperities and creates a reduction in localized contact pressure.

2.4.3.4 Affecting the fluid drag and viscosity

Under hydrodynamic lubrication conditions, where two rubbing surfaces are fully separated by a hydrodynamic flow, viscosity is the dominating factor in the friction force and load-bearing capacity of the lubricant. The viscosity of a lubricant is dependent on fluid flow and fluid drag, so any additive that can affect these two factors may be effective in hydrodynamic lubrication condition. Under a normal load, 2D nanomaterials align orderly in the fluid direction leading to decreased momentum transfer between adjacent fluid layers and reduction in viscosity [48].

3. EXPERIMENTAL DETAIL

3.1 Materials

Commercialized Ti_3C_2 flakes with 99.9% purity (Wuhan Golden Wing Industry & Trade, Wuhan, China) with the nominal size of the flakes was 0.2 μm − 3 μm. Fig 13 (a) shows SEM images of Ti_3C_2 flakes. It can be seen from Fig. 13 (a) that the lateral size of Ti_3C_2 flakes varied from less than 1 μm to several μm. The high-magnification SEM image inset in Fig. 13 (a) shows clearly the layered structure of Ti_3C_2. In addition, the thickness of the layer was found to be approximately 20 nm, which was consistent with the thickness reported in literature [29,32]. The XRD patterns of the Ti_3C_2 powders in shows that the typical diffraction peak (002) of Ti_3C_2 appears at around $2\theta = 8.98^o$, indicating that the formation of Ti_3C_2 which was accomplished by selectively removing Al from Ti_3AlC_2, through the disappearance of the strongest diffraction peak of Ti_3AlC_2 at $2\theta = 39^o$ [54]. Five solutions with different concentrations of Ti_3C_2 in pure deionized (DI) water were prepared as showed in Fig. 13 (b) with an aim of investigating the effect of concentration on friction and wear characteristics. To prepare the solutions, 0.01 g, 0.02 g, 0.03 g, 0.05 g, and 0.07 g of Ti_3C_2 was added to 1 ml of DI water for the solutions with 1 wt%, 2 wt%, 3 wt%, 5 wt%, and 7 wt% Ti_3C_2 concentrations, respectively. Then, each solution was stirred in a magnetic stirrer for 1 hour at room temperature to ensure that Ti_3C_2 was uniformly dispersed.

Martensitic SS (AISI 440C) was selected as the ball material due to its high hardness and corrosion resistance in water. The nominal radius of the balls was 3 mm. All balls used in this work were carefully examined under a LSCM (VK-X200, Keyence, Osaka, Japan) to determine the radii and to assess their surfaces before experiment. Figure 13 (c) shows a photograph of the ball glued on the holder for the experiment, along with an example of the three-dimensional (3D) LSCM image before experiment. The average radius of the balls was calculated to be 3.02 ± 0.01 mm (mean ± one standard deviation). It can be seen from Fig. 13 (c) that the surface of the ball before experiment was quite clean. The average surface roughness (R_a) of the balls was also determined from the LSCM data with a scan size of 1,270 μm × 997 μm after the flattening process. The R_a value of the balls was calculated to be 0.29 ± 0.01 μm. The hardness of the balls was further determined using a micro-Vickers hardness tester (MMT-7, Matsuzawa, Japan). To that end, a ball was ground to form a flat surface. Hardness measurement was

performed with an indentation force of 0.98 N and dwell time of 20 s at five different randomly selected locations of three balls. The hardness values of the three balls were found to be similar to one another (765 ± 28 HV, 785 ± 34 HV, and 730 ± 10 HV). The average hardness value was determined to be 760 ± 23 HV. The hardness values of the balls determined in this work were in a good agreement with those of AISI 440C SS.

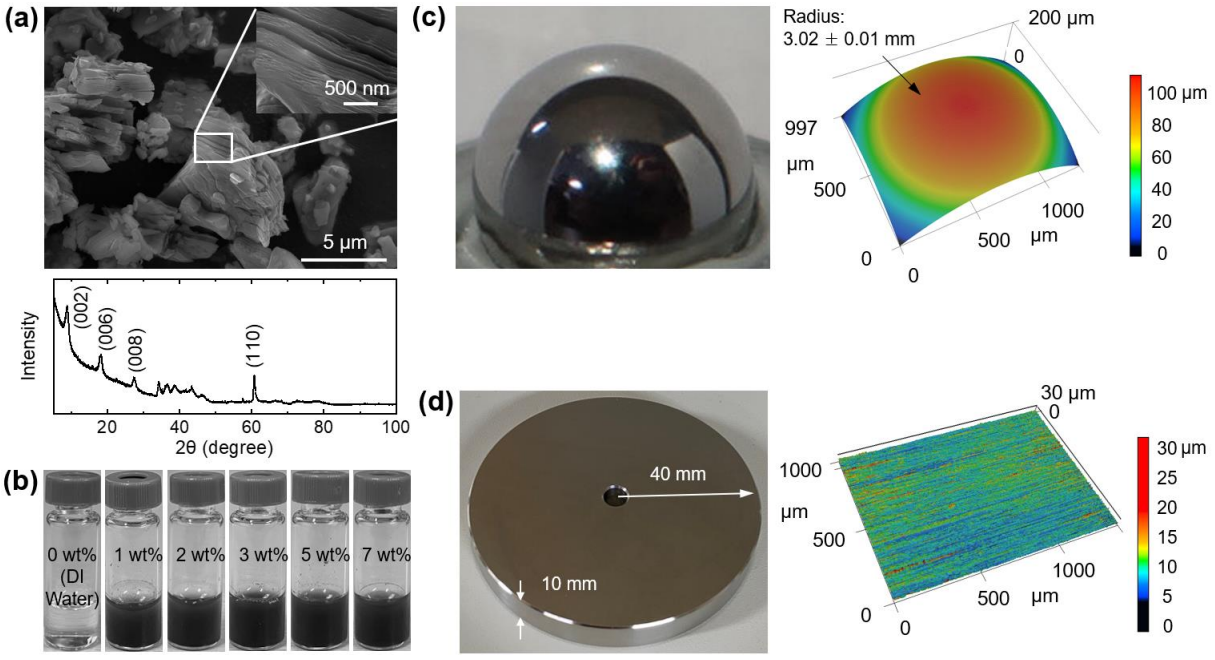

Figure 13. (a) SEM images and XRD pattern of Ti_3C_2 flakes before test, (b) photographs of water-based lubricants with 0 wt%, 1 wt%, 2 wt%, 3 wt%, 5 wt%, and 7 wt% Ti_3C_2 concentrations, and photographs and 3D LSCM images of (c) ball and (d) disk. Inset in (a) is a high-magnification of the SEM image

Austenitic SS (AISI 304) was used as the disk material. SS disks with a radius of 40 mm and a thickness of 10 mm were prepared for the experiment. Figure 13 (d) shows the photograph and 3D LSCM image of a disk before experiment. From Fig. 13 (d), the patterns, which likely formed during the manufacturing process, can be observed. The value of R_a of the disks was determined to be 1.67 ± 0.05 μm from the LSCM data with a scan size of 1,408 μm × 1,056 μm obtained at five different locations on five different disks. The hardness of the disks was measured from five different locations of five disks using the micro-Vickers hardness tester with an indentation force of 0.98 N and dwell time

of 20 s. The average hardness value of the disks was 220 ± 10 HV, which was within the typical range of hardness of AISI 304 SS.

3.2 Methods

The tribological properties of the Ti_3C_2 as water-based lubricant additives for contact sliding between a SS ball and a disk were investigated using a ball-on-disk tribotester under boundary lubrication. A photograph of the tester used in this work is shown in Fig. 14. A normal force was applied by dead weight and the friction force was monitored using a load cell equipped with the tester. The experiments were conducted for a specimen radius of 10 mm at a constant rotating speed of 120 rpm, hence the linear sliding speed was calculated to be 0.126 m/s. The normal force varied from 3 N to 10 N, which corresponded to a contact pressure from 0.91 to 1.36 GPa, as calculated using Hertzian contact model [46]. The experiment with a given normal force was conducted for up to 7,000 cycles corresponding to the sliding distance of one cycle was 0.063 m, and 0.2 ml of lubricant was applied to the contact area using a syringe. The lubricants were supplied right after the preparation to minimize the effect of dispersibility of additives on the experimental results. The experiments were repeated at least three times for each experimental condition. Prior to the experiment, the balls and disks were cleaned with isopropyl alcohol (IPA) by ultrasonication for 1 hour. All tests were performed in ambient conditions with the temperature 24°C − 26°C and relative humidity 37 − 46%.

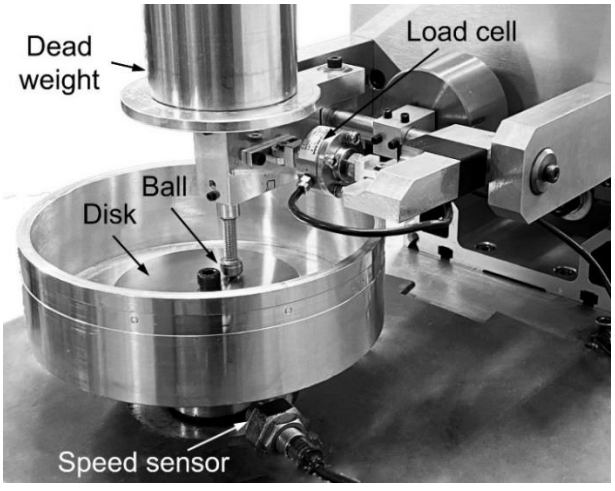

Figure 14. Photograph of the ball-on-disk tribotester used in this work.

The surface of the balls and the wear track formed on the disks were carefully examined after experiments using the LSCM to understand the wear characteristics of water-based lubricants with Ti_3C_2 additives. In particular, the degree of ball and disk wear were quantitatively determined using Archard's wear law [55]. To that end, additional LSCM images of the balls and disks were acquired after the ultrasonic cleaning since a significant amount of wear debris and additives may have been readily deposited on the surfaces during the experiment. The wear volume of the balls was determined as the volume of the spherical segment calculated using the cross-sectional height profiles at the center of the ball before and after experiment, considering that the ball was flattened due to wear. As for the disks, the LSCM images were obtained at five different locations of the wear track and the averaged cross-sectional height profiles were taken from each image. Then, the wear volume of the disk was calculated by multiplying the average cross-sectional area of the wear track by the circumferential contact length. Furthermore, SEM observations and Energy-dispersive X-ray spectroscopy (EDS) analysis were performed, particularly of Ti_3C_2 flakes after the experiment, to gain a better understanding of tribological behavior of water-based lubricants with Ti_3C_2 additives.

4. RESULTS AND DISCUSSION

4.1 Friction characteristics

Figure 15 (a) shows the variation of friction coefficient with the number of cycles under a 3 N normal force obtained using the water lubricants with 0 wt%, 1 wt%, 2 wt%, 3 wt%, 5 wt%, and 7 wt% Ti_3C_2 concentrations. The initial friction coefficient was found to range from 0.17 to 0.31. Also, it was shown that the friction coefficient fluctuated during the initial stage of contact sliding for up to 3,000 cycles. Then, the friction coefficient became relatively stable, and ranged from 0.24 to 0.34, as the Ti_3C_2 concentration varied from 0 wt% to 7 wt%. It is plausible that the friction coefficient varies during the run-in process and become stable with increasing the number of cycles [56]. The difference in the variation of friction coefficient during the run-in period can be observed, which was likely associated associated with various factors such as initial states of ball and disk surface and initial amount of Ti_3C_2 at the contacting interface. In general, it was observed that the friction increased and then decreased during run-in process. Given that such behavior may be associated with the ball flattening. At the initial state of contact sliding, contact area may relatively small, and therefore, the entrance of Ti_3C_2 flake may be limited. However, more flakes may be readily captured at the contacting interfaces as the ball become flattened. It is plausible that the friction coefficient varies during the run-in process and become stable with increasing the number of cycles [56]. The data presented in Fig. 15 (a) show that the friction coefficients for the water lubricants with Ti_3C_2 additives were consistently lower than that without Ti_3C_2 additives. It can also be seen from the figure that the decrease in friction coefficient was the largest when the Ti_3C_2 concentration was 5 wt%. The friction coefficients were averaged after they became stable (*i.e.*, from 3,000 to 7,000 cycles) for a clear comparison, and the variation of average friction coefficient was plotted against the Ti_3C_2 concentration under various normal forces, as shown in Fig. 15(b). It can be observed from the figure that the friction coefficient generally decreased as the Ti_3C_2 concentration increased up to 5 wt%, but it increased when the Ti_3C_2 concentration was 7 wt%, as anticipated from the data in Fig. 15 (a). However, the effect of normal force on friction coefficient was not clearly observed. The friction coefficients for 0 wt% and 5 wt% Ti_3C_2 concentrations were found to range from 0.29 to 0.33 and from 0.20 to 0.26, respectively. The decrease in the friction coefficient for a 5 wt%

Ti_3C_2 concentration was calculated to be approximately 13% − 31%, compared to that for a 0 wt.% Ti_3C_2 concentration.

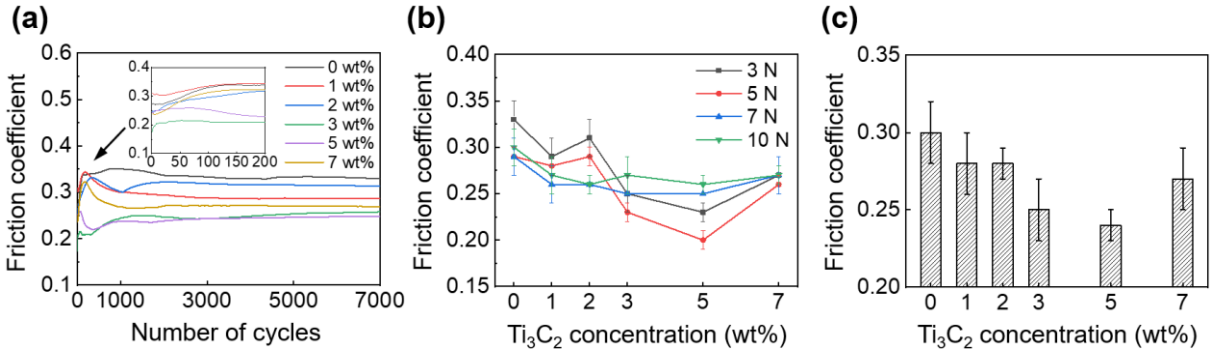

Figure 15. (a) Variation of friction coefficient with the number of cycles under 3 N normal force, (b) variation of friction coefficient at steady state with Ti_3C_2 concentration under 3N – 10 N normal force, and (c) variation of average friction coefficient with Ti_3C_2 concentration. Inset in (a) is the plot of friction coefficient for the number of cycles below 200.

The friction coefficients obtained for normal forces ranging from 3 N to 10 N were further averaged to investigate more carefully the effect of Ti_3C_2 concentration, as shown in Fig. 15 (c). It was found that the friction coefficients decreased by 7%, 7%, 17%, 20%, and 10% for 1 wt%, 2 wt%, 3 wt%, 5 wt%, and 7 wt% Ti_3C_2 concentrations, respectively, compared to the friction coefficient for a 0 wt% Ti_3C_2 concentration. These observations clearly suggest that Ti_3C_2 can reduce friction between a SS ball and a SS disk as an additive for water-based lubrication. The decrease in friction may be associated with behavior of Ti_3C_2 (*e.g.*, adherence to surface and trapping in grooves) that enter into the contacting interface, as proposed in previous studies [29-32]. Also, it can be concluded that the optimal concentration of Ti_3C_2 for friction reduction was 5 wt% for the considered material pair and experimental conditions adopted for this work. The friction reduction effect may likely decrease when an excess Ti_3C_2 is applied to the contact interface (*e.g.*, Ti_3C_2 concentration larger than 5 wt.%), as consistently observed in previous investigations [29-32]. The degree of friction reduction by Ti_3C_2 for water-based lubrication was relatively smaller than that offered by graphene-based materials [17,18]. However, the decrease in the friction provided by Ti_3C_2 was comparable with those offered by other 2D

materials, such as h-BN [22] and MoS_2 [23] in water-based lubrication. Interestingly, the friction reduction obtained with Ti_3C_2 for oil-based lubrication [29-32] is generally smaller than when using graphene-based materials [57,58], but comparable to those offered by h-BN [59] and MoS_2 [60]. It should further be noted that the degree of friction reduction by additives may significantly vary depending on experimental conditions. Nevertheless, the overall results in Fig. 15 clearly suggest the feasibility of using Ti_3C_2 as an additive for water-based lubrication.

4.2 Wear characteristics

The wear characteristics of the balls and disks were assessed to elucidate further the feasibility of Ti_3C_2 as a water-based lubrication additive. Figure 16 (a) shows 3D LSCM images of the balls cleaned using IPA after the experiments under a 3 N normal force. As examples, the images of the ball tested using the water lubricants with 0 wt%, 1 wt% and 5 wt% Ti_3C_2 concentrations are shown in Fig. 16 (a). In Fig. 16 (a), the cross-sectional height profiles before and after the experiment are provided for clear observation of wear. It can be seen from the figure that the balls were generally flattened due to the wear. Also, it was observed that slight scratches appeared on the ball surface along the sliding direction. The ball wear volumes and wear rates for various normal forces are plotted as functions of Ti_3C_2 concentration in Figs. 16 (b) and (c), respectively. The ball wear volume ranged from $(6.4 \pm 1.6) \times 10^{-4}$ mm^3 to $(3.7 \pm 1.6) \times 10^{-3}$ mm^3 under 3 N – 10 N normal forces with 0 wt% – 7 wt% Ti_3C_2 concentrations. No clear effect of the normal force on the ball wear volume was observed in Fig. 16 (b). Additionally, it was shown that the effect of Ti_3C_2 concentration on the wear volume was not significant under a given normal force. The ball wear rate was calculated to be from $(1.0 \pm 0.3) \times 10^{-8}$ $mm^3/(N \cdot cycle)$ to $(13 \pm 3.7) \times 10^{-8}$ $mm^3/(N \cdot cycle)$ under 3 N – 10 N normal forces with 0 wt% – 7 wt% Ti_3C_2 concentrations, as shown in Fig. 16 (c). As predicted from the data shown in Fig. 16 (b), no significant dependence of the wear rate on the normal force and Ti_3C_2 concentration was further observed. This result suggests that the ball wear did not progress enough for the effects of normal force and Ti_3C_2 concentration to be observed clearly. The variation of average ball wear rate with Ti_3C_2 concentration is plotted in Fig. 16 (d) for clarity. The ball wear rate with 1 wt% – 7 wt% Ti_3C_2 concentrations were slightly larger than that with 0 wt% Ti_3C_2 concentration within the experimental uncertainties. As expected, the effect of

Ti_3C_2 concentration on the ball wear rate was not significant. This result might be feasibly associated with the higher hardness of the ball than that of the disk, which resulted in the suppression of ball wear. A long-term test would be preferable for clear observation of the effects of normal force and Ti_3C_2 concentration on the ball wear.

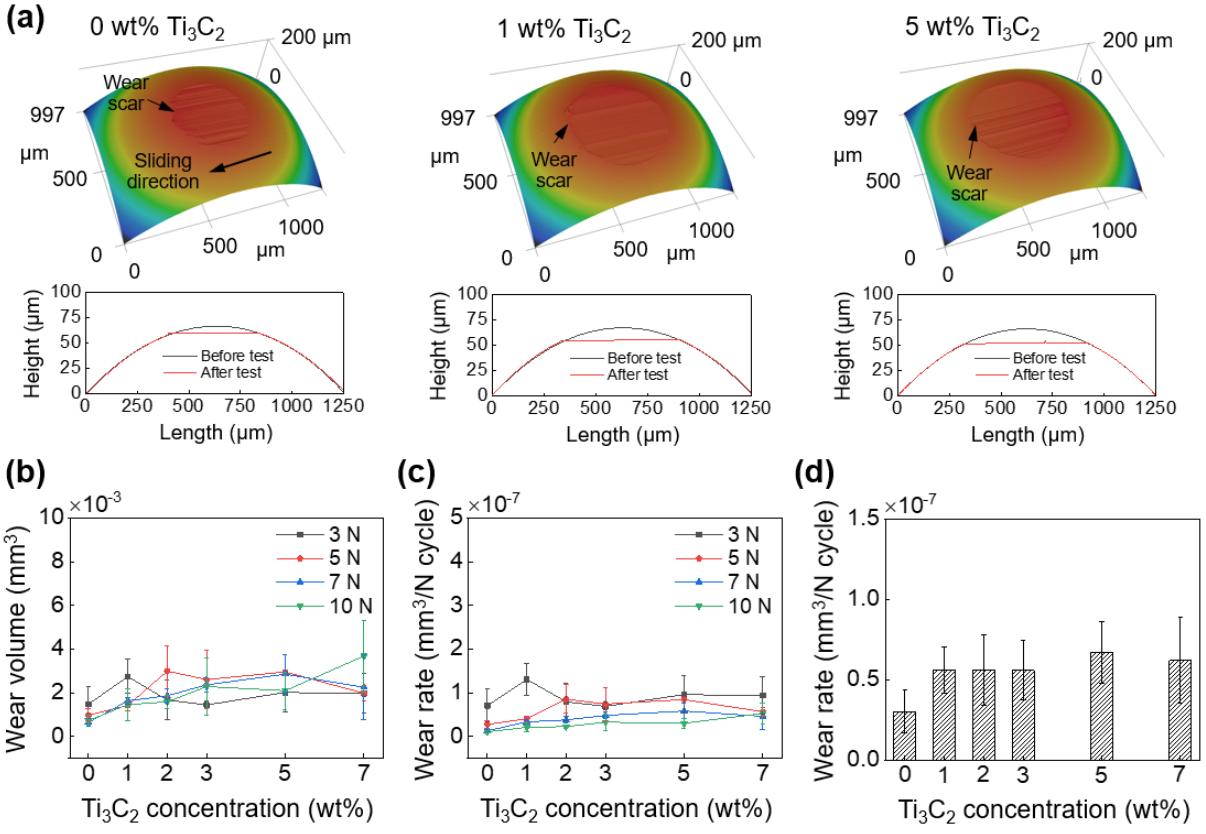

Figure 16. (a) 3D LSCM images and cross-sectional height profiles of balls after experiments with 0 wt%, 1 wt%, and 5 wt% Ti_3C_2 concentrations under 3 N normal force, (b) variation of ball wear volume and (c) wear rate under 3N – 10 N normal force with Ti_3C_2 concentration, and (d) variation of average wear rate with Ti_3C_2 concentration. In (a), cross-sectional profiles before experiments are included for comparison.

Figure 17 (a) shows the LSCM images of the wear tracks formed on the disks after the experiments under a 3 N normal force for varying Ti_3C_2 concentrations. The averaged cross-sectional height profiles of the wear tracks are also presented in Fig. 17 (a). The data in Fig. 17 (a) were obtained after the IPA cleaning. The images in Fig. 17 (a) demonstrate clearly that a significant amount of scratches were

formed along the sliding direction on all disks. It was observed from the data in Fig. 17 (a) that in general, the effect of Ti_3C_2 concentration on the depth of the wear track was not consistent (depth of 1.64 µm, 0.6 µm, 1.49 µm, 0.52 µm, 0.50 µm, and 0.68 µm for 0 wt%, 1 wt%, 2 wt%, 3 wt%, 5 wt%, and 7 wt% Ti_3C_2 concentration, respectively). However, it can clearly be seen that the width of the wear track significantly decreased as the Ti_3C_2 concentration increased up to 5 wt% (width of 452.0 µm, 371.2 µm, 340.2 µm, 275.0 µm, and 236.6 µm for 0 wt%, 1 wt%, 2 wt%, 3 wt%, and 5 wt% Ti_3C_2 concentration, respectively). Subsequently, the width of the wear track was found to increase (341.3 µm) when the Ti_3C_2 concentration increased to 7 wt%. The width of the wear track was expected to increase as the flattened area of the ball increased. However, no significant relationship between the flattened width of the ball and the width of the wear track on disk was observed from Figs. 16 (a) and 15 (a). For example, although the flattened width of the ball after experiment with a 7 wt% Ti_3C_2 concentration was larger than that after the experiment with 0 wt.% Ti_3C_2 (Fig. 16 (a)), the wear track was wider for 0 wt% Ti_3C_2 concentration than that for 7 wt% Ti_3C_2 concentration (Fig. 17 (a)). These results indicate that the direct contact between the ball and disk may be hindered by Ti_3C_2 flakes, particularly at the edges of the contact interface, and that such hindering by Ti_3C_2 flakes was more substantial as Ti_3C_2 concentration increased up to 5 wt%. However, it was postulated that this behavior of Ti_3C_2 flakes mitigated when an excessive amount of Ti_3C_2 flakes (*e.g.*, 7 wt%.) was applied to contact interface.

The variation of disk wear volume with Ti_3C_2 concentration is presented in Fig. 17 (b). The wear volume of the disks ranged from $(1.9 \pm 0.6) \times 10^{-2}$ mm^3 to $(5.1 \pm 0.3) \times 10^{-2}$ mm^3 as the normal force varied from 3 N to 10 N and the Ti_3C_2 concentration from 0 wt.% to 7 wt.%. Similar to the wear of the balls, the effect of normal force on the disk wear volume was not clearly observed. However, it can be seen that the disk wear volume generally decreased as the Ti_3C_2 concentration increased to 5 wt% and then increased when Ti_3C_2 concentration was 7 wt%, as expected from the data presented in Fig. 17 (a). The decrease in the wear volume for 5 wt% Ti_3C_2 concentration (1.9×10^{-2} mm^3) was as high as 55% under a 3 N of normal force, compared to the wear volume for 0 wt% Ti_3C_2 concentration (4.3×10^{-2} mm^3).

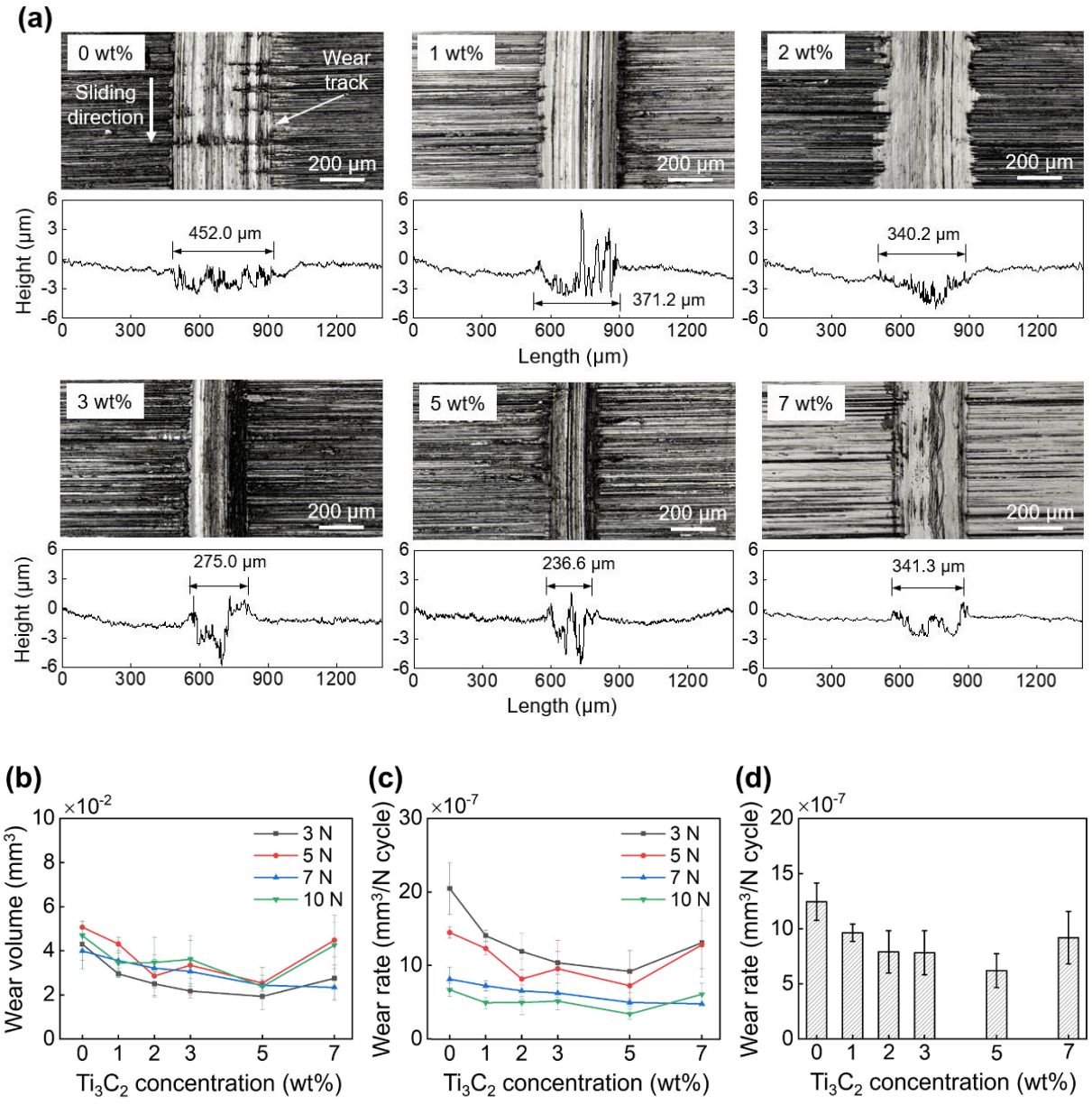

Figure 17. (a) LSCM images and cross-sectional height profiles of disks after experiments with 0 wt%, 1 wt%, 2 wt%, 3 wt%, 5 and 7 wt% Ti_3C_2 concentrations under 3 N normal force, (b) variation of disk wear volume and (c) wear rate under 3N – 10 N normal force with Ti_3C_2 concentration, and (d) variation of average wear rate with Ti_3C_2 concentration.

Figure 17 (c) shows the variation of disk wear rate for a given normal force with Ti_3C_2 concentration. It can be seen in the figure that the wear rate decreased with increasing normal force. For example, as the normal force increased from 3 N to 10 N, the wear rates for 0 wt% and 5 wt% Ti_3C_2 concentrations decreased from $(20 \pm 3.5) \times 10^{-7}$ $mm^3/(N \cdot cycle)$ to $(6.7 \pm 0.9) \times 10^{-7}$ $mm^3/(N \cdot cycle)$ and from $(9.2 \pm 2.9) \times 10^{-7}$ $mm^3/(N \cdot cycle)$ to $(3.4 \pm 0.7) \times 10^{-7}$ $mm^3/(N \cdot cycle)$, respectively. Ti_3C_2 flakes may be more damaged due to interactions with ball, disk and other Ti_3C_2 flakes under higher normal force. However, this may contribute to enhanced formation of a tribo-film that can suppress wear progression [29-32], which could be one of the reasons for the low wear rate under high normal force. In general, the wear rate was found to decrease with increasing Ti_3C_2 concentration from 0 wt% to 5 wt%, and then increase when Ti_3C_2 concentration was higher than 5 wt%. To clearly examine the effect of Ti_3C_2 concentration on the disk wear rate, the average wear rates for a given concentration are shown in Fig. 17 (d). The wear rates were calculated to be $(12 \pm 1.7) \times 10^{-7}$ $mm^3/(N \cdot cycle)$, $(9.6 \pm 0.8) \times 10^{-7}$ $mm^3/(N \cdot cycle)$, $(7.9 \pm 1.9) \times 10^{-7}$ $mm^3/(N \cdot cycle)$, $(7.8 \pm 2.0) \times 10^{-7}$ $mm^3/(N \cdot cycle)$, $(6.2 \pm 1.5) \times 10^{-7}$ $mm^3/(N \cdot cycle)$, and $(9.2 \pm 2.4) \times 10^{-7}$ $mm^3/(N \cdot cycle)$ for Ti_3C_2 concentrations of 0 wt%, 1 wt%, 2 wt%, 3 wt%, 5 wt%, and 7 wt%, respectively. The decrease in wear rates for 1 wt%, 2 wt%, 3 wt%, 5 wt%, and 7 wt% Ti_3C_2 concentrations was calculated to be 20%, 34%, 35%, 48%, and 23%, respectively, compared to the wear rate for 0 wt% Ti_3C_2 concentration. Decrease in the disk wear rate for 5 wt% Ti_3C_2 concentration is relatively large, compared to that provided by h-BN [22], while it is relatively small, compared to that offered by graphene-based materials [17,18] for water-based lubrication. It is interesting to note that for oil-based lubrication the decrease in the wear rate provided by Ti_3C_2 [29,32] is often smaller than that provided by other 2D materials, including graphene-based materials, h-BN and MoS_2 [57-60]. Nonetheless, the overall results presented in Fig. 17 along with the data in Fig. 15 demonstrate the feasibility of Ti_3C_2 as a water-based lubrication additive for wear reduction.

To gain a better understanding of the effect of Ti_3C_2 on wear, the balls and disks were carefully examined before they were cleaned. As examples, the high-magnification LSCM images obtained after experiments with 0 wt%, 1 wt%, 5 wt% and 7 wt% Ti_3C_2 concentrations are shown in Figs. 18 (a), (b), (c), and (d), respectively. From images in Fig. 18 (a), along with those in Figs. 16 and 17, signs of

abrasive and adhesive wear can be observed on both the ball and disk surfaces after the experiment with 0 wt% Ti_3C_2 concentration. However, the disk wear was more severe than the ball wear, which was due to the fact that the hardness of the disk was significantly smaller than that of the ball. In addition, the slight occurrence of abrasive wear was observed on the ball, which may be associated with the hard wear particles at the contact interface [41]. Figure 18 (a) also shows the wear debris adhered to both the ball and disk surfaces. It was likely that the wear debris on the ball and disk surfaces was mainly generated from the disk, considering the disk wear volume was one or two orders of magnitude larger than the ball wear volume.

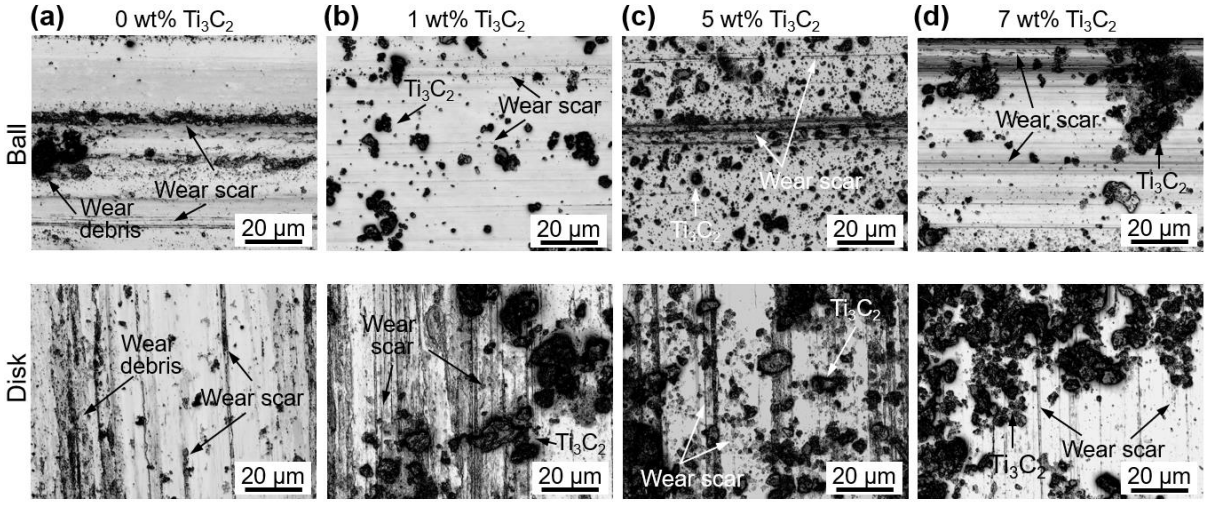

Figure 18. LSCM images of the flattened area of ball and wear track of disk after experiments with (a) 0 wt%, (b) 1 wt%, (c) 5 wt%, and (d) 7 wt% Ti_3C_2 concentrations under 3 N normal force.

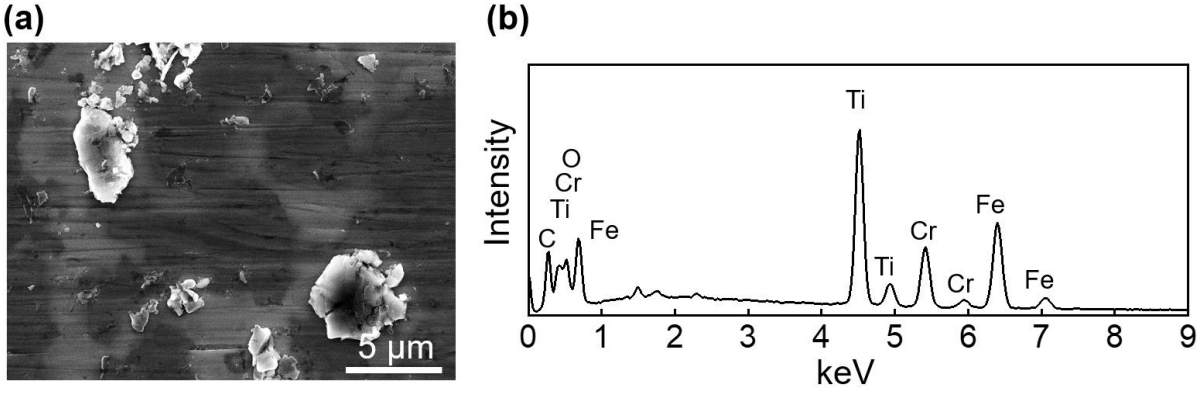

Figure 19. Examples of SEM image and EDS spectrum of Ti_3C_2 on the flattened area of ball

Figure 18 shows that the amount of particles on both the ball and disk surfaces generally increased with increasing Ti_3C_2 concentration. These particles were expected to be mostly Ti_3C_2 given that the wear volume of ball and disk was a few orders of magnitude smaller than the volume of Ti_3C_2 in lubricant. SEM image and EDS spectrum of these particles on the ball surface are provide in Fig.19. The planar shape of the particles and the relatively strong Ti peak clearly indicate that these particles were mainly Ti_3C_2. The planar shape of Ti_3C_2 may be advantageous for it to enter the contact interface. It is likely that the Ti_3C_2 flakes on the contact interface could hinder the direct contact between the ball and disk, leading to suppression of wear progression [29]. Particularly, this behavior of Ti_3C_2 was expected to be more significant at the edges of the contact area, as discussed earlier. It can also be seen that Ti_3C_2 was relatively well scattered on both the ball and disk surfaces with 5 wt% concentration (Fig. 18 (c)) than for 1 wt% concentration (Fig. 18 (b)). This may be responsible for more significant wear reduction as Ti_3C_2 concentration increased up to 5 wt%. However, it can be seen from Fig. 18 (d) that Ti_3C_2 was more agglomerated after the experiment for 7 wt% Ti_3C_2 concentration. Such agglomeration can be clearly observed from the SEM image of Ti_3C_2 after the experiment, shown in Fig. 20 and the data of flakes size analysis in Fig. 21. Comparing Figs. 13 (a) and data showing from Fig. 21, the lateral size of the flakes from less than 1 μm to several μm as showed in Fig. 13 (a). Assume that the flakes were circle, the flake area can be determined less than ten square micrometers. However, the flake area of Ti_3C_2 was found to increase up to several tens of square micrometer after test due to agglomeration. Given that the agglomeration can come from the wear debris. However, Ti_3C_2 volumes correspond with 0.2 ml lubricant delivered to the contact area were 0.48 (mm^3), 0.95 (mm^3), 1.43 (mm^3), 2.38 (mm^3) and 3.32 (mm^3) with 1 wt%, 2 wt%, 3 wt%, 5 wt% and 7 wt% Ti_3C_2 concentration, respectively. Comparison with the wear volume of the ball and disk in Fig. 16 (b) and Fig. 17 (b), can be concluded that the agglomeration from the Ti_3C_2 flakes because the volume of Ti_3C_2 is much larger than wear volume of the ball and disk. It was plausible that more significant agglomeration of Ti_3C_2 at its high concentration may be responsible for the mitigation of the wear suppression effect, as proposed in the previous study [57]. Figure 22 shows SEM images of Ti_3C_2 and a tribo-film formed on the ball surface after experiments with 7 wt% Ti_3C_2 concentration under 10 N normal force. The data in Fig. 22 suggest the damage of

Ti_3C_2 and the formation of tribo-film under relatively high normal force, which may contribute to suppressing the wear progression, as discussed earlier. It should further be noted that Ti_3C_2 can readily be oxidized in water, especially from the edges of the flakes, and TiO_2 can be formed [61,62]. Hence, as a result of oxidation, the layered structure of Ti_3C_2 could be degraded, which may lead to a further decrease in its performance as an additive. However, such a performance decrease could be partly compensated, given that TiO_2 may be used as a lubricant additive [12].

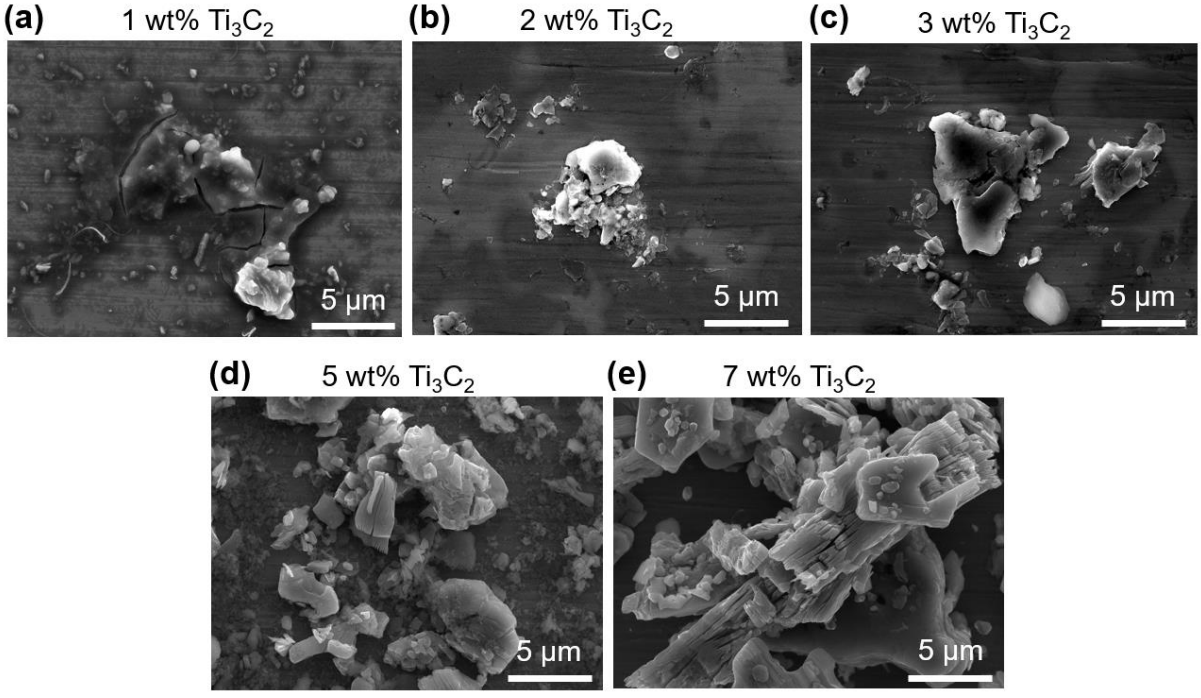

Figure 20. SEM images of the agglomerated Ti_3C_2 on the flattened area of ball after experiments with (a) 1 wt%, (b) 2 wt%, (c) 3 wt%, (d) 5 wt% and (e) 7 wt% Ti_3C_2 concentrations under 10 N normal force.

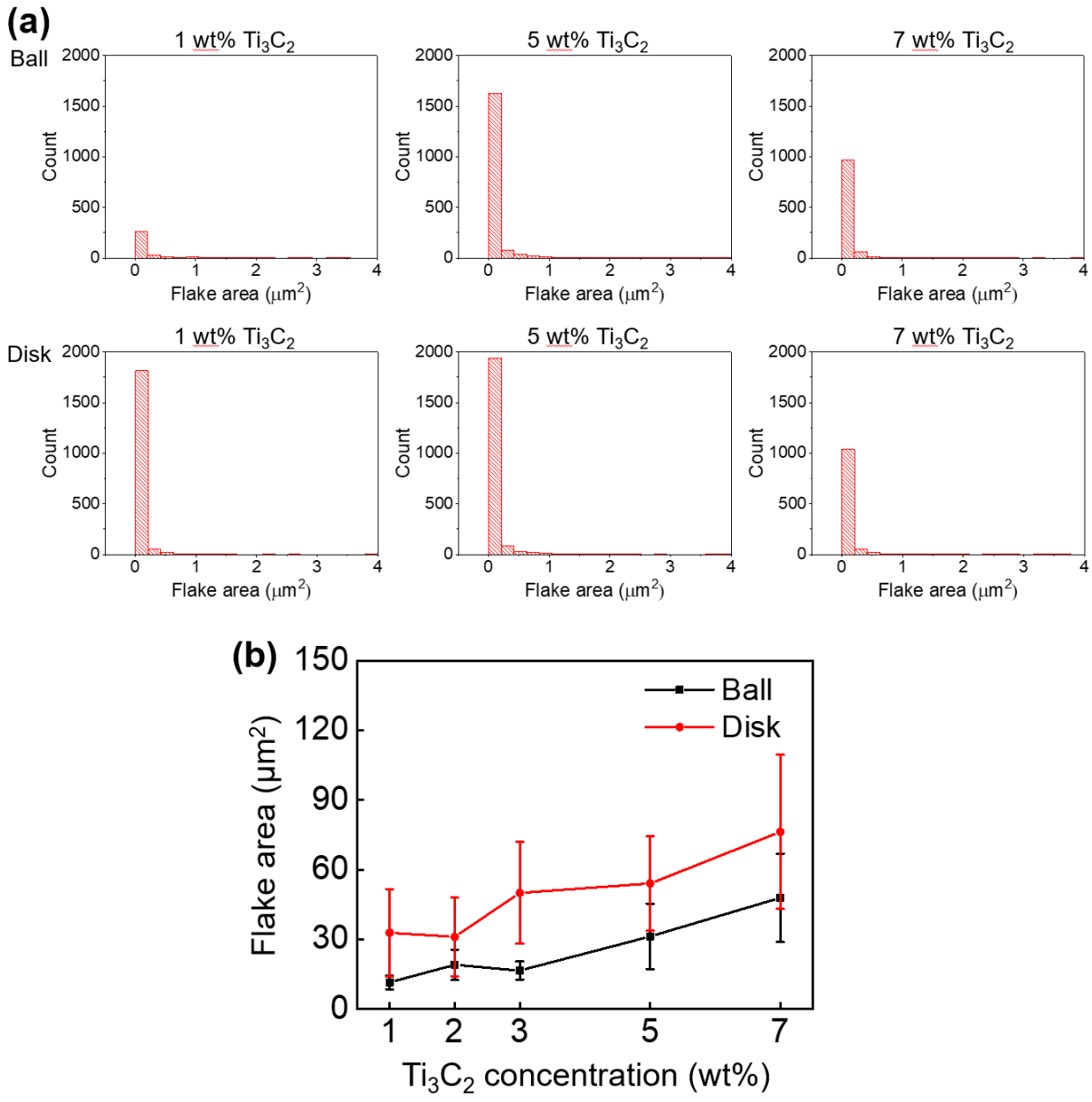

Figure 21. (a) Distribution of flake size on flattened area of ball and wear track of disk with 1 wt%, 5 wt% and 7 wt%, (b) flakes size analysis of Ti_3C_2 on the flattened area of ball and disk after experiments under 10 N normal force.

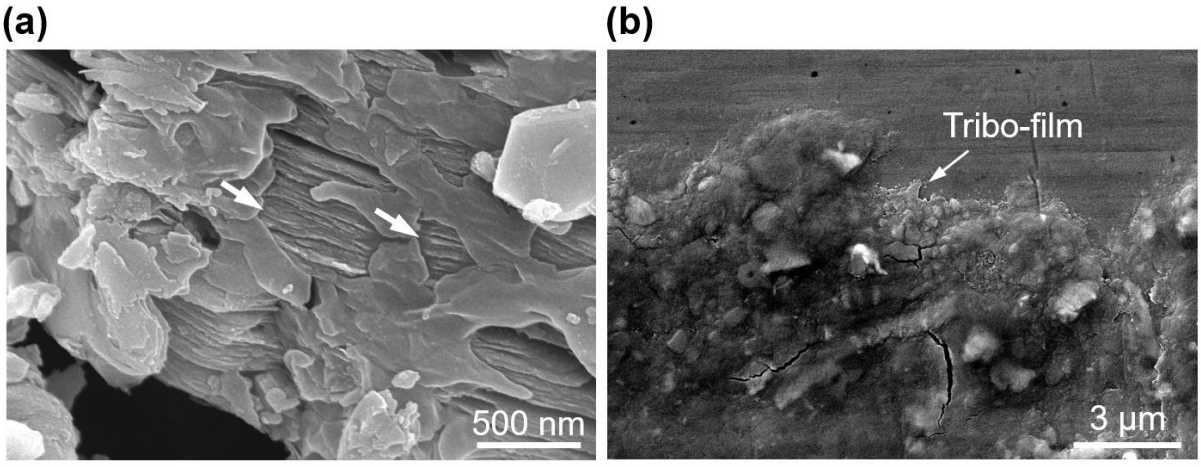

Figure 22. SEM images of (a) Ti_3C_2 and (b) tribofilm on the flattened area of ball surface after experiment with 7 wt% Ti_3C_2 concentrations under 10 N normal force.

It should be noted that the tribological characteristics may vary significantly, depending on material pair and operating and environmental conditions. Hence, the studies across a broad spectrum of experimental parameters are needed to elucidate the feasibility of Ti_3C_2 as an additive for water-based lubrication. In particular, a database to determine the optimal concentration should be established, given that optimal concentrations of lubricant additives may be dependent on the tribological system. The effect of size, thickness, and functional group on the tribological characteristics should be explored to improve the performance of water-based lubrication. Long-term tests are further needed for the practical applicability of Ti_3C_2 as a lubricant additive. Nevertheless, the results of this work provide useful information for the fundamental tribological properties of Ti_3C_2 as a feasible water-based lubrication additive.

5. CONCLUSIONS AND RECOMMENDATION

5.1 Conclusions

In this work, the friction and wear characteristics of Ti_3C_2 as an additive for water-based lubrication were experimentally assessed using a ball-on-disk tribotester. The experiments were performed using SS balls and disks at varying normal forces and Ti_3C_2 concentrations. The overall results show that Ti_3C_2 can provide friction and wear reduction for water-based lubrication. The decrease in the direct contact between the ball and the disk offered by Ti_3C_2 flakes was believed to be responsible for this outcome. It was also shown that the hindering of contact was more significant at the edges of the contact interface, which in turn led to suppression of wear progression. Additionally, the degrees of reduction of friction and wear were found to increase from 7% to 20% and from 20% to 48%, respectively, as Ti_3C_2 concentration increased from 1 wt% to 5 wt%, compared to the friction and wear without Ti_3C_2 additive. However, the reduction in friction and wear were limited to 10% and 23%, respectively, when Ti_3C_2 concentration further increased to 7 wt%. The excessive agglomeration of Ti_3C_2 flakes may be responsible for this outcome. The results of this work may provide useful information for a fundamental understanding of the tribological properties of Ti_3C_2 as a water-based lubrication additive and may therefore aid developing environment-friendly lubricants.

5.2 Recommendation and future works

Based on the limitations of this work, several recommendations were made for further investigation. Firstly, long term test to evaluate the suitability of the data over a long period of time should be performed. Secondly, many factors such as sliding speed, temperature, and environmental conditions may affect the optimal value of Ti_3C_2, and then the tribological behavior of Ti_3C_2 may vary depending on the tribological system. Therefore, the experiment across broad spectrum of experimental parameters is needed. Finally, the comparison tribological properties of Ti_3C_2 as lubricant additive in water with other 2-D materials should be performed to investigate the prominence of Ti_3C_2 in 2-D family.

REFERENCES

1. Nosonovsky, M.; Bhushan, B. Green tribology: principles, research areas and challenges. *Philos Trans A Math Phys Eng Sci* **2010**, *368*, 4677-4694, doi:10.1098/rsta.2010.0200.
2. de Kraker, A.; van Ostayen, R.A.J.; Rixen, D.J. Calculation of Stribeck curves for (water) lubricated journal bearings. *Tribology International* **2007**, *40*, 459-469, doi:10.1016/j.triboint.2006.04.012.
3. Gao, G.; Yin, Z.; Jiang, D.; Zhang, X. Numerical analysis of plain journal bearing under hydrodynamic lubrication by water. *Tribology International* **2014**, *75*, 31-38, doi:10.1016/j.triboint.2014.03.009.
4. Ohana, T.; Suzuki, M.; Nakamura, T.; Tanaka, A.; Koga, Y. Low-friction behaviour of diamond-like carbon films in a water environment. *Diamond and Related Materials* **2006**, *15*, 962-966, doi:10.1016/j.diamond.2005.12.008.
5. Wang, Q.; Zhou, F.; Wang, X.; Chen, K.; Wang, M.; Qian, T.; Li, Y. Comparison of tribological properties of CrN, TiCN and TiAlN coatings sliding against SiC balls in water. *Applied Surface Science* **2011**, *257*, 7813-7820, doi:10.1016/j.apsusc.2011.04.035.
6. Ding, Q.; Wang, L.; Wang, Y.; Wang, S.C.; Hu, L.; Xue, Q. Improved Tribological Behavior of DLC Films Under Water Lubrication by Surface Texturing. *Tribology Letters* **2010**, *41*, 439-449, doi:10.1007/s11249-010-9730-1.
7. Yamakiri, H.; Sasaki, S.; Kurita, T.; Kasashima, N. Effects of laser surface texturing on friction behavior of silicon nitride under lubrication with water. *Tribology International* **2011**, *44*, 579-584, doi:10.1016/j.triboint.2010.11.002.
8. Chen, C.-Y.; Wu, B.-H.; Chung, C.-J.; Li, W.-L.; Chien, C.-W.; Wu, P.-H.; Cheng, C.-W. Low-Friction Characteristics of Nanostructured Surfaces on Silicon Carbide for Water-Lubricated Seals. *Tribology Letters* **2013**, *51*, 127-133, doi:10.1007/s11249-013-0153-7.
9. Tomala, A.; Karpinska, A.; Werner, W.S.M.; Olver, A.; Störi, H. Tribological properties of additives for water-based lubricants. *Wear* **2010**, *269*, 804-810, doi:10.1016/j.wear.2010.08.008.

10. Zhang, C.; Zhang, S.; Song, S.; Yang, G.; Yu, L.; Wu, Z.; Li, X.; Zhang, P. Preparation and Tribological Properties of Surface-Capped Copper Nanoparticle as a Water-Based Lubricant Additive. *Tribology Letters* **2014**, *54*, 25-33, doi:10.1007/s11249-014-0304-5.

11. Alias, A.A.; Kinoshita, H.; Fujii, M. Tribological properties of diamond nanoparticle additive in water under a lubrication between steel plate and tungsten carbide ball. *Journal of Advanced Mechanical Design, Systems, and Manufacturing* **2015**, *9*, JAMDSM0006-JAMDSM0006, doi:10.1299/jamdsm.2015jamdsm0006.

12. Wu, H.; Zhao, J.; Xia, W.; Cheng, X.; He, A.; Yun, J.H.; Wang, L.; Huang, H.; Jiao, S.; Huang, L., et al. A study of the tribological behaviour of TiO 2 nano-additive water-based lubricants. *Tribology International* **2017**, *109*, 398-408, doi:10.1016/j.triboint.2017.01.013.

13. Bao, Y.Y.; Sun, J.L.; Kong, L.H. Tribological properties and lubricating mechanism of SiO2 nanoparticles in water-based fluid. *IOP Conference Series: Materials Science and Engineering* **2017**, *182*, doi:10.1088/1757-899x/182/1/012025.

14. Jiang, G.; Yang, Y. Preparation and tribology properties of water-soluble fullerene derivative nanoball. *Arabian Journal of Chemistry* **2017**, *10*, S870-S876, doi:10.1016/j.arabjc.2012.12.022.

15. Peng, Y.; Hu, Y.; Wang, H. Tribological behaviors of surfactant-functionalized carbon nanotubes as lubricant additive in water. *Tribology Letters* **2006**, *25*, 247-253, doi:10.1007/s11249-006-9176-7.

16. Berman, D.; Erdemir, A.; Sumant, A.V. Graphene: a new emerging lubricant. *Materials Today* **2014**, *17*, 31-42, doi:10.1016/j.mattod.2013.12.003.

17. Kinoshita, H.; Nishina, Y.; Alias, A.A.; Fujii, M. Tribological properties of monolayer graphene oxide sheets as water-based lubricant additives. *Carbon* **2014**, *66*, 720-723, doi:10.1016/j.carbon.2013.08.045.

18. Xie, H.; Jiang, B.; Dai, J.; Peng, C.; Li, C.; Li, Q.; Pan, F. Tribological Behaviors of Graphene and Graphene Oxide as Water-Based Lubricant Additives for Magnesium Alloy/Steel Contacts. *Materials (Basel)* **2018**, *11*, doi:10.3390/ma11020206.

19. Ky, D.L.C.; Khac, B.C.T.; Le, C.T.; Kim, Y.S.; Chung, K.H. Friction characteristics of mechanically exfoliated and CVD-grown single-layer MoS2. *Friction* **2018**, *6*, 395-406, doi:10.1007/s40544-017-0172-8.

20. Tran Khac, B.C.; DelRio, F.W.; Chung, K.H. Interfacial Strength and Surface Damage Characteristics of Atomically Thin h-BN, MoS2, and Graphene. *ACS Appl Mater Interfaces* **2018**, *10*, 9164-9177, doi:10.1021/acsami.8b00001.

21. Tran-Khac, B.C.; Kim, H.J.; DelRio, F.W.; Chung, K.H. Operational and environmental conditions regulate the frictional behavior of two-dimensional materials. *Appl Surf Sci* **2019**, *483*, doi:10.1016/j.apsusc.2019.03.249.

22. Cho, D.-H.; Kim, J.-S.; Kwon, S.-H.; Lee, C.; Lee, Y.-Z. Evaluation of hexagonal boron nitride nano-sheets as a lubricant additive in water. *Wear* **2013**, *302*, 981-986, doi:10.1016/j.wear.2012.12.059.

23. Zhang, B.M.; Sun, J.L. Tribological performances of multilayer-MoS2nanoparticles in water-based lubricating fluid. *IOP Conference Series: Materials Science and Engineering* **2017**, *182*, doi:10.1088/1757-899x/182/1/012023.

24. Anasori, B.; Lukatskaya, M.R.; Gogotsi, Y. 2D metal carbides and nitrides (MXenes) for energy storage. *Nature Reviews Materials* **2017**, *2*, doi:10.1038/natrevmats.2016.98.

25. Zhang, D.; Ashton, M.; Ostadhossein, A.; van Duin, A.C.T.; Hennig, R.G.; Sinnott, S.B. Computational Study of Low Interlayer Friction in Tin+1Cn (n = 1, 2, and 3) MXene. *ACS Appl Mater Interfaces* **2017**, *9*, 34467-34479, doi:10.1021/acsami.7b09895.

26. Lian, W.; Mai, Y.; Liu, C.; Zhang, L.; Li, S.; Jie, X. Two-dimensional Ti3C2 coating as an emerging protective solid-lubricant for tribology. *Ceramics International* **2018**, *44*, 20154-20162, doi:10.1016/j.ceramint.2018.07.309.

27. Rosenkranz, A.; Grützmacher, P.G.; Espinoza, R.; Fuenzalida, V.M.; Blanco, E.; Escalona, N.; Gracia, F.J.; Villarroel, R.; Guo, L.; Kang, R., et al. Multi-layer Ti3C2Tx-nanoparticles (MXenes) as solid lubricants – Role of surface terminations and intercalated water. *Applied Surface Science* **2019**, *494*, 13-21, doi:10.1016/j.apsusc.2019.07.171.

28. Marian, M.; Tremmel, S.; Wartzack, S.; Song, G.; Wang, B.; Yu, J.; Rosenkranz, A. Mxene nanosheets as an emerging solid lubricant for machine elements – Towards increased energy efficiency and service life. *Applied Surface Science* **2020**, *523*, doi:10.1016/j.apsusc.2020.146503.

29. Liu, Y.; Zhang, X.; Dong, S.; Ye, Z.; Wei, Y. Synthesis and tribological property of Ti3C2T X nanosheets. *Journal of Materials Science* **2016**, *52*, 2200-2209, doi:10.1007/s10853-016-0509-0.

30. Xue, M.; Wang, Z.; Yuan, F.; Zhang, X.; Wei, W.; Tang, H.; Li, C. Preparation of TiO2/Ti3C2Tx hybrid nanocomposites and their tribological properties as base oil lubricant additives. *RSC Advances* **2017**, *7*, 4312-4319, doi:10.1039/c6ra27653a.

31. Yang, J.; Chen, B.; Song, H.; Tang, H.; Li, C. Synthesis, characterization, and tribological properties of two-dimensional Ti3C2. *Crystal Research and Technology* **2014**, *49*, 926-932, doi:10.1002/crat.201400268.

32. Zhang, X.; Xue, M.; Yang, X.; Wang, Z.; Luo, G.; Huang, Z.; Sui, X.; Li, C. Preparation and tribological properties of Ti3C2(OH)2 nanosheets as additives in base oil. *RSC Advances* **2015**, *5*, 2762-2767, doi:10.1039/c4ra13800g.

33. Hailing, J. Friction and wear transitions of materials. *Wear* **1991**, *142*, 387-388, doi:10.1016/0043-1648(91)90177-v.

34. Blau, P.J. Interpretations of the friction and wear break-in behavior of metals in sliding contact. *Wear* **1981**, *71*, 29-43, doi:10.1016/0043-1648(81)90137-x.

35. Blau, P.J. *Friction Science and Technology: From Concepts to Applications*; CRC Press: 2008.

36. Furey, M.J. Surface Temperatures in Sliding Contact. *A S L E Transactions* **1964**, *7*, 133-146, doi:10.1080/05698196408972043.

37. Rabinowicz, E. Lubrication of metal surfaces by oxide films. *Wear* **1968**, *11*, 389-390, doi:10.1016/0043-1648(68)90697-2.

38. Kenneth, H., et al. *Triboscience and tribotechnology superior friction and wear control in engines and transmissions. Scientific Report: European Cooperation in Science and Technology*; European Cooperation in Science and Technology: Brussels, Belgium., 2007.

39. Buckley, D.H. Possible relation of friction of copper-aluminium alloys with decreasing stacking-fault energy. *Wear* **1968**, *11*, doi:10.1016/0043-1648(68)90198-1.

40. He, Y.J.; Winnubst, A.J.A.; Schipper, D.J.; Bakker, P.M.V.; Burggraaf, A.J.; Verweij, H. Friction and wear behaviour of ceramic-hardened steel couples under reciprocating sliding motion. *Wear* **1995**, *184*, 33-43, doi:10.1016/0043-1648(94)06544-6.

41. Rabinowicz, E. *Friction and Wear of Materials*, 2nd ed.; John Wiley & Sons: New York, USA, 1995; pp. 124-142.

42. Cizichos, H. *Tribology: A systems approach to the science and technology of friction, lubrication and wear* Elsevier, Academic Press: New York, USA 1978; Vol. 1 pp. 417.

43. G W Stachowiak, A.W.B. *Engineering tribology*; Oxford: Butterworh-Heinemann: USA, 2014; pp. 883.

44. George E Totten, S.R.W., Rajesh J Shah. *Fuels and lubricants handbook : technology, properties, performance, and testing*; ASTM International: USA, 2003; pp. 1087.

45. Rizvi, S.Q.A. *A comprehensive review of lubricant chemistry, technology, selection, and design*; ASTM International: USA, 2009; pp. 674.

46. Hertz, H.R. Ueber die Berührung fester elastischer Körper. *Journal für die reine und angewandte Mathematik (Crelles Journal)* **1882**, *1882*, 156-171, doi:10.1515/crll.1882.92.156.

47. Bhushan, B. *Modern tribology handbook, two volume set* 1ed.; CRC Press: New York, USA 2000; pp. 1728.

48. Xiao, H.; Liu, S. 2D nanomaterials as lubricant additive: A review. *Materials & Design* **2017**, *135*, 319-332, doi:10.1016/j.matdes.2017.09.029.

49. Berman, D.; Erdemir, A.; Sumant, A.V. Few layer graphene to reduce wear and friction on sliding steel surfaces. *Carbon* **2013**, *54*, 454-459, doi:10.1016/j.carbon.2012.11.061.

50. Berman, D.; Erdemir, A.; Sumant, A.V. Reduced wear and friction enabled by graphene layers on sliding steel surfaces in dry nitrogen. *Carbon* **2013**, *59*, 167-175, doi:10.1016/j.carbon.2013.03.006.

51. Naguib, M.; Kurtoglu, M.; Presser, V.; Lu, J.; Niu, J.; Heon, M.; Hultman, L.; Gogotsi, Y.; Barsoum, M.W. Two-dimensional nanocrystals produced by exfoliation of Ti3 AlC2. *Adv Mater* **2011**, *23*, 4248-4253, doi:10.1002/adma.201102306.

52. Naguib, M.; Mashtalir, O.; Carle, J.; Presser, V.; Lu, J.; Hultman, L.; Gogotsi, Y.; Barsoum, M.W. Two-dimensional transition metal carbides. *ACS Nano* **2012**, *6*, 1322-1331, doi:10.1021/nn204153h.

53. Naguib, M.; Halim, J.; Lu, J.; Cook, K.M.; Hultman, L.; Gogotsi, Y.; Barsoum, M.W. New two-dimensional niobium and vanadium carbides as promising materials for Li-ion batteries. *J Am Chem Soc* **2013**, *135*, 15966-15969, doi:10.1021/ja405735d.

54. Feng, A.; Yu, Y.; Wang, Y.; Jiang, F.; Yu, Y.; Mi, L.; Song, L. Two-dimensional MXene Ti3C2 produced by exfoliation of Ti3AlC2. *Materials & Design* **2017**, *114*, 161-166, doi:10.1016/j.matdes.2016.10.053.

55. Hirst, J.F.A.a.W. The wear of metals under unlubricated conditions. *Proceedings of the Royal Society of London. Series A. Mathematical and Physical Sciences* **1956**, *236*, 397-410, doi:10.1098/rspa.1956.0144.

56. Blau, P.J. On the nature of running-in. *Tribology International* **2005**, *38*, 1007-1012, doi:10.1016/j.triboint.2005.07.020.

57. Guo, Y.-B.; Zhang, S.-W. The Tribological Properties of Multi-Layered Graphene as Additives of PAO2 Oil in Steel–Steel Contacts. *Lubricants* **2016**, *4*, doi:10.3390/lubricants4030030.

58. Wu, P.; Chen, X.; Zhang, C.; Zhang, J.; Luo, J.; Zhang, J. Modified graphene as novel lubricating additive with high dispersion stability in oil. *Friction* **2020**, 10.1007/s40544-019-0359-2, doi:10.1007/s40544-019-0359-2.

59. Çelik, O.N.; Ay, N.; Göncü, Y. Effect of Nano Hexagonal Boron Nitride Lubricant Additives on the Friction and Wear Properties of AISI 4140 Steel. *Particulate Science and Technology* **2013**, *31*, 501-506, doi:10.1080/02726351.2013.779336.

60. Mousavi, S.B.; Heris, S.Z.; Estelle, P. Experimental comparison between ZnO and MoS2 nanoparticles as additives on performance of diesel oil-based nano lubricant. *Sci Rep* **2020**, *10*, 5813, doi:10.1038/s41598-020-62830-1.

61. Zhang, C.J.; Pinilla, S.; McEvoy, N.; Cullen, C.P.; Anasori, B.; Long, E.; Park, S.-H.; Seral-Ascaso, A.; Shmeliov, A.; Krishnan, D., et al. Oxidation Stability of Colloidal Two-Dimensional Titanium Carbides (MXenes). *Chemistry of Materials* **2017**, *29*, 4848-4856, doi:10.1021/acs.chemmater.7b00745.

62. Ghassemi, H.; Harlow, W.; Mashtalir, O.; Beidaghi, M.; Lukatskaya, M.R.; Gogotsi, Y.; Taheri, M.L. In situ environmental transmission electron microscopy study of oxidation of two-dimensional Ti3C2and formation of carbon-supported TiO2. *Journal of Materials Chemistry A* **2014**, *2*, doi:10.1039/c4ta02583k.